Journal of Medicinal Chemistry

pubs.acs.org/jmc

Article

G-Quadruplex DNA as a Target in Pathogenic Bacteria: Efficacy of an Extended Naphthalene Diimide Ligand and Its Mode of Action

Published as part of the Journal of Medicinal Chemistry special issue "Epigenetics 2022".

Rubén Cebrián,*,⊥ Efres Belmonte-Reche,⊥ Valentina Pirota,⊥ Anne de Jong, Juan Carlos Morales, Mauro Freccero, Filippo Doria,* and Oscar P. Kuipers*

Cite This: *J. Med. Chem.* 2022, 65, 4752−4766

Read Online

ACCESS | Metrics & More | Article Recommendations | Supporting Information

ABSTRACT: Guanidine DNA quadruplex (G4-DNA) structures convey a distinctive layer of epigenetic information that is critical for regulating key biological activities and processes as transcription, replication, and repair in living cells. The information regarding their role and use as therapeutic drug targets in bacteria is still scarce. Here, we tested the biological activity of a G4-DNA ligand library, based on the naphthalene diimide (NDI) pharmacophore, against both Gram-positive and Gram-negative bacteria. For the best compound identified, **NDI-10**, a different action mechanism was described for Gram-positive or negative bacteria. This asymmetric activity profile could be related to the different prevalence of putative G4-DNA structures in each group, the influence that they can exert on gene expression, and the different roles of the G4 structures in these bacteria, which seem to promote transcription in Gram-positive bacteria and repress transcription in Gram-negatives.

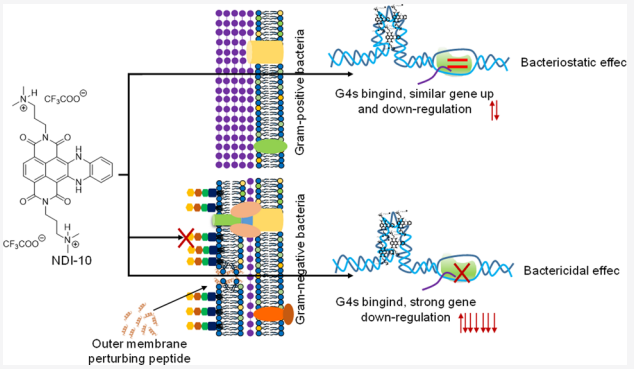

INTRODUCTION

Antimicrobial drug resistance is a natural process expedited by the widespread misuse and extensive use of antibiotics, which pose a threat for the global healthcare systems.[1,2] To treat the increasing number of antimicrobial-resistant bacteria (AMR), very few new clinically relevant antibiotics have been approved in the last years.[3] Most are derivatives of previously approved antibiotics and offer a short time solution, since the resistance mechanisms against them are already established in nature.[4,5] With this background, global health care is facing new challenges to treat infectious diseases, as, without effective drugs, even the most simple surgical process can become problematic. New drugs with innovative action mechanisms and/or targets and the absence of cross-resistance with traditional antibiotics are therefore necessary.[6,7]

In this context, G-quadruplex structures (G4s) of DNA or RNA represent some of the most important secondary structures in nucleic acids that play a key role in several biological processes like transcription, replication, and translation.[8,9] G4s can be defined as highly ordered DNA and RNA stable secondary structures found in G-rich nucleic acid sequences, wherein guanine bases are associated via hydrogen bonds to form G-tetrads that stack in a planar arrangement with a stabilizing monovalent cation occupying a central position in the cavity.[10] The first proposed consensus sequence for these motifs was $G_{3+}N_{1-7}G_{3+}N_{1-7}G_{3+}N_{1-7}G_{3+}$,[8,11] although nonabiding quadruplexes have been identified with smaller G-runs,[12] longer loops, and bulges within the runs.[13] Structurally, G4s can be formed by one, two, or four separate strands of DNA (or RNA) and can be arranged following a wide variety of topologies depending on the combinations of strand directions as well as variations in loop size, sequence, or cation concentrations.[14] G4s have been extensively studied as targets in cancer research, because of their presence in regulatory regions of cancer-related genes[15−17] as well as being possible targets in viruses[18−20,9,21] and more recently in parasites.[22,23] However, the information regarding the G4s presence and function in bacteria is still scarce, as is the possibility of using G4s as novel antimicrobial targets.[24−26]

According to the G-Quadruplex Ligands Database (G4LDB), almost 1000 G4 ligands that have been synthesized and characterized can induce, stabilize, and bind DNA or RNA G4s.[27,28] Among these, naphthalene diimides (NDIs)[29] stand

Received: November 5, 2021
Published: December 20, 2021

https://doi.org/10.1021/acs.jmedchem.1c01905
J. Med. Chem. 2022, 65, 4752−4766

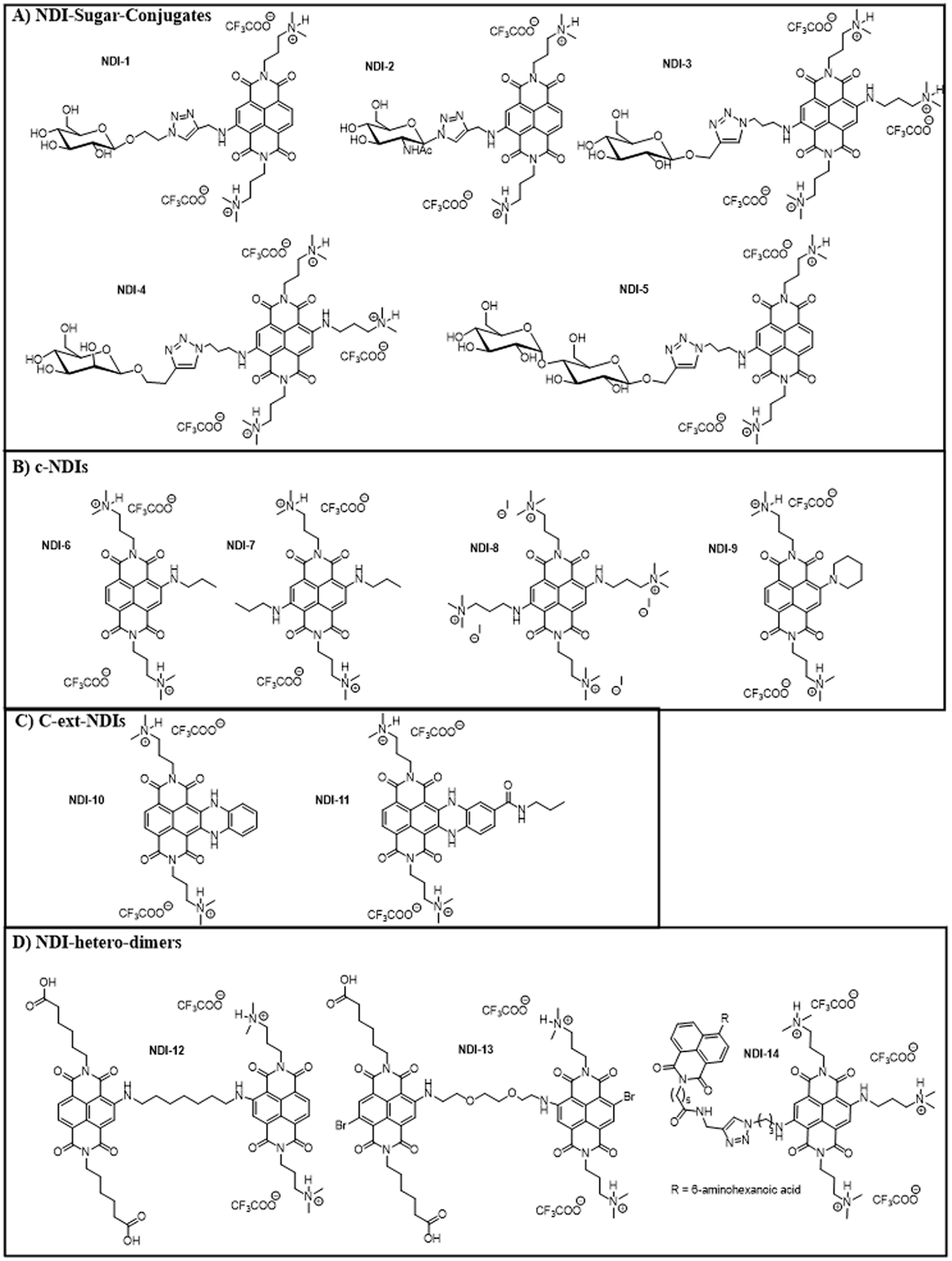

Figure 1. Chemical structures of (A) NDI-Sugar conjugates (**NDI-1−5**), (B) core-substituted NDIs (c-NDIs; **NDI-6−9**), (C) core-extended NDI (C-ext-NDIs; **NDI-10** and **NDI-11**), and (D) NDI-heterodimers (**NDI-12−14**) synthesized and investigated in the present study.

out as very interesting pharmacophores because of their ability to interact with different G4s. Their unique optoelectronic properties, combined with their flexible synthetic protocols, which allow a relatively easy chemical modification of four

https://doi.org/10.1021/acs.jmedchem.1c01905
J. Med. Chem. 2022, 65, 4752−4766

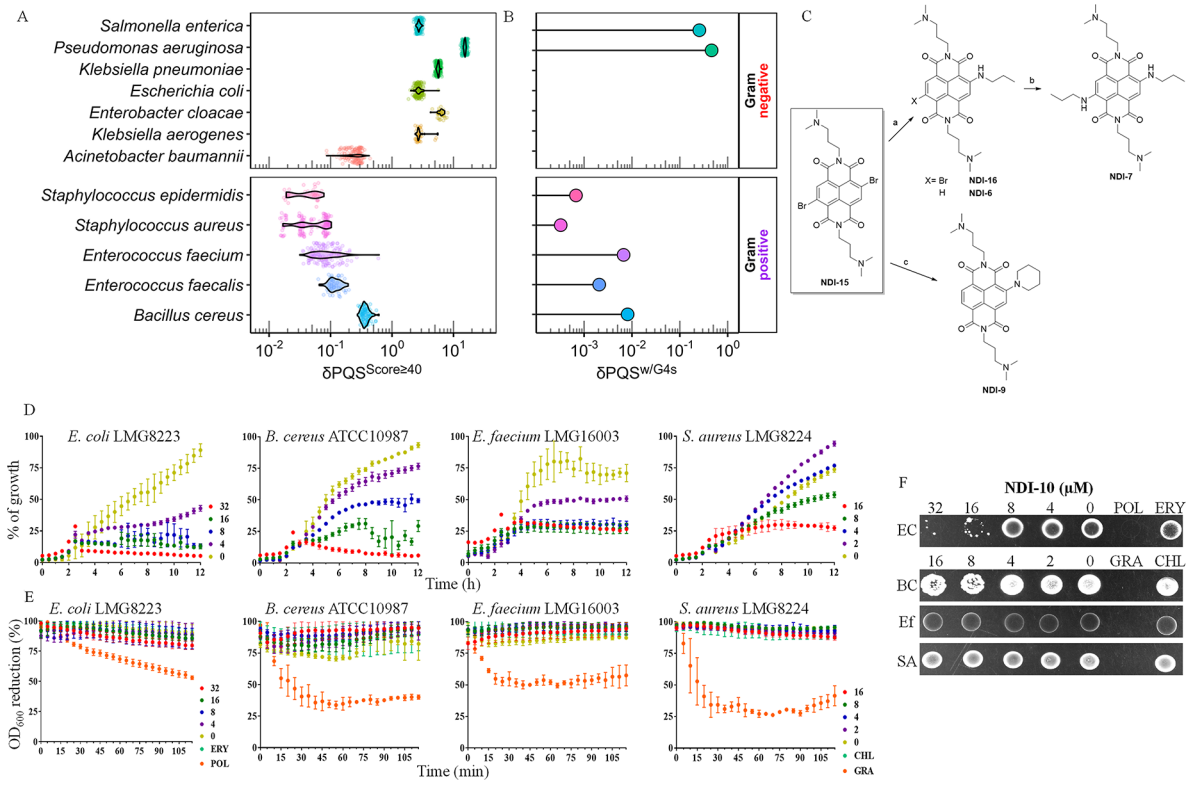

Figure 2. (A) Density of PQS with a high probability of forming G4 (per 100 000 nucleotides and bacteria). (B) Mean density of candidates with already confirmed G4 (per 100 000 nucleotides and bacteria). (C) Synthesis of **NDI-7** and **NDI-9**: (a) **NDI-15** with 4.0 equiv of 1-aminopropane in CH_3CN, reflux, 1 h; (b) **NDI-16** as a mixture in neat 1-aminopropane, 150 °C, 10 min, closed-vessel MW-assisted (250 psi); (c) **NDI-15** with 3.0 equiv of piperidine in CH_3CN, reflux, 2 h. (D) Effect of **NDI-10** when added to growing cell cultures **NDI-10** concentrations are expressed in micromolar units. (E) Bacteriolytic activity of **NDI-10** (no effect was observed). ERY, erythromycin (32 μM), POL, Polymyxin B (2 μM), CHL, chloramphenicol (16 μM), and GRA, gramicidin S (4 μM). (F) Bacteriostatic/bactericidal activity for **NDI-10**. EC, *E. coli* LMG 8223, BC, *B. cereus* ATCC 10987, Ef, *E. faecium* LMG 16003, SA, *S. aureus* LMG 8224.

different side chains on the aromatic core or in imidic positions, make them one of the most studied G4 binders. Such a structural diversification can be exploited to implement the binding affinity, water solubility, thermal stability, and cellular uptake.[29] In parallel, the NDI core extension[30] offers the opportunity to improve G4s binding and selectivity by increasing the large electron-poor planar aromatic surface that guarantees an effective π-stacking on top of the terminal G-tetrads. All these features prompted different research groups to design and investigate several NDI derivatives that were active and selective toward various forms of cancer[31−34] and viral[35,36] or parasite[22,37] infections.

The main aim of the present work is to evaluate the antimicrobial activity of a small library of 14 newly synthesized or known NDIs, grouped in four different classes of NDIs (Figure 1A−D), against several Gram-negative and Gram-positive bacteria that are currently listed as priority pathogens by the WHO and for which new and effective drugs are necessary.[7] The action mechanism of the best G4-ligand candidate found (**NDI-10**) was analyzed under several conditions. A biophysics evaluation of G4-ligands interaction with six selected putative G4 sequences of *Escherichia coli* and *Staphylococcus aureus* highlighted the potential of **NDI-10** in the stabilizing ability through these G4 structures. Moreover, its in vivo activity in a *Galleria mellonella* infection model and its hemolytic activity were determined.

RESULTS AND DISCUSSION

In Silico Identification of Potential G4s in Bacterial Genomes. A broad in silico analysis using several bacterial genomes of the pathogenic strains considered in this work was first executed to explore the presence and distribution of potential G4 sequences (PQSs). In total, 1222 bacterial genomes categorized into 12 species (seven Gram-negative and five Gram-positive) were analyzed using the R-package G4-iM Grinder (G4-iM Grinder, Figure 2, Supporting Information 1).[38] The results were filtered by their quadruplex formation potential score (Score ≥ |40|), to keep only the sequences most probable to form G4s. The PQS density per species was calculated as numbers of PQS per 100 000 nucleotides (Figure 2A), to compare different sized genomes. The presence and density of sequences already confirmed to form G4 within the candidates were also analyzed for the bacterial genomes used (Figure 2B, Supporting Information 1).

The results and their interspecies average showed obvious differences between the 12 bacteria. Most of the Gram-negative genomes can be grouped by their particularly dense PQS prevalence, of which *Pseudomonas aeruginosa* had overwhelmingly the densest occurrence of those examined, with a genome very rich in candidates in relation to the rest of the bacteria. The other Gram-negative genomes presented relatively high prevalences as well, except *Acinetobacter baumannii,* which showed a significant reduction in candidates, with a number of PQS similar to the ones found in *Bacillus cereus* (having the densest genome of those examined in Gram-

https://doi.org/10.1021/acs.jmedchem.1c01905
J. Med. Chem. 2022, 65, 4752−4766

positive bacteria). The Gram-positive bacteria presented fewer PQS candidates, highlighting the *Staphylococcus* genus, which was less dense in potential G4s.

For the bacteria studied, the GC% (where G = guanine and C = cytosine) genomic content between Gram-positive and Gram-negative bacteria was found to be related to the putative-G4 presence. However, the relationship between GC content and PQS presence was not linear, and other factors such as the genomic organization or the GC distribution in the genome may also play a key role in the presence of potential G4s. In fact, when put in context with the widely studied human genome, the density of highly probable G4 candidates prevalence in *P. aeruginosa* was less than half of that determined in the human genome (15 vs 40), while the GC % content in the bacteria was ∼66% versus ∼40% in humans.

For all the bacterial species analyzed here, at least some specific strains were identified to contain in their genomes already confirmed G4 sequences in vitro under specific cation concentrations and/or pH conditions. Although they were found to be independent of the PQS density (δPQS) in the genome, they do depend on the G4-database used to match the candidates (no direct relation between the in silico δPQS with score greater than 40 and the presence of confirmer G4s can be established with the currently available data). Hence, future G4-database updates will expand the known G4s found in these bacterial genomes. For the current version of the G4-database used, we identified in the Gram-negative *Salmonella enterica* 18 already confirmed and unique G4s, including KRAS (utr-1 and 2),[39] TERF2,[40] and PAR21,[41] among others (Supporting Information 2). For *Pseudomonas aeruginosa,* 29 unique G4s were found, including KRAS (utr-1 and 2), Tet22,[41] and 6C.C0.[42] Other Gram-negative bacteria presented lower densities of confirmed G4s and only in a few of the many strains analyzed (Supporting Information 2). When taking into account all the strains analyzed, the average densities for these Gram-negative bacteria were found to be extremely low. For the Gram-positive bacteria, an intermediate number of unique known G4s were detected, which were in all cases associated with long tracks of repeating Gs (2G_L0 and 3G_L0,[43] EPL.G and [GGGG]4[44]) (Figure 2B, Supporting Information 2).

Our results show apparent differences between Gram-positive and Gram-negative bacteria. However, these differences are not uniformly distributed within the groups, as other factors such as the genus and species seem also to influence the prevalence of PQSs. For example, *Acinetobacter baumannii* presented a prevalence of PQS that was overall more characteristic of Gram-positive bacteria than Gram-negative bacteria. These results are in agreement with a previous literature comparison, where Gram-negative bacteria were found to be denser in PQS than Gram-positive,[38] yet some specific genus such as *Mycobacterium* (Gram-positive bacteria) was found to be denser in PQS than any of those analyzed here, while *Legionella pneumophila* was found to be very poor in candidates despite being a Gram-negative bacterium.

Although this situation needs further clarification, the present search identified several confirmed G4s in the genome of all the bacterial species, besides many more candidates with a high probability of forming G4s. These (confirmed and potential) G4s are hence therapeutic targets that can now be targeted with G4-ligands as potential antibiotics.

G4-Ligand Synthesis. To perform our study, we focused the attention on four different classes of NDI derivatives: (a) five NDI sugar conjugates (**NDI-1−5**, Figure 1A), (b) four di- and tetracationic core-substituted NDIs (**NDI-6−9**, Figure 1B), (c) two core-extended NDIs (**NDI-10** and **NDI-11**, Figure 1C), and (d) three hetero NDI-dimers (**NDI-12−14**, Figure 1D). The NDIs chosen are characterized by high chemical diversity, for evaluating the effects on antimicrobial activity depending on different core substitutions, the extension of the aromatic core, dimeric binding units, or a carbohydrate conjugation. The only common feature, which is kept similar within the families, are two side chains at the imide position with fixed length and bearing physiologically charged terminal moiety ($NHMe_2^+$), an essential characteristic for cell permeability. **NDI-1−6**,[37,45] **NDI-8**,[46] and **NDI-10−14**,[31,32,47,48] selected from our in-house library, have been previously synthesized and characterized. **NDI-7** and **NDI-9** are novel ligands that have been obtained following a common synthetic protocol starting from **NDI-15**, which was prepared as reported previously[49] (Figure 2C). **NDI-7** was synthesized in two steps, using 1-aminopropane for both nucleophilic aromatic substitutions (SNAr). The first reaction was performed in refluxing acetonitrile, and an excess of amines resulted in a competitive dehalogenation of the precursor and product, yielding both the brominated **NDI-16** and the dehalogenated product **NDI-6**. A second microwave-assisted SNAr step was performed by using 1-aminopropane as a solvent, yielding **NDI-7** as a pure blue solid. The same protocol was applied to prepare **NDI-9**, replacing 1-aminopropane with piperidine as the reactant of the first SNAr.

Antimicrobial Activity of NDIs. The NDIs compounds were diluted in dimethyl sulfoxide (DMSO) to 10 mM, and then they were tested at concentrations ranging from 128 to 2 μM by serial dilutions in 96-well plates according to the Clinical and Laboratory Standards Institute (CLSI) specifications.[50] From the initial 14 compounds, only 2 showed antimicrobial activity (**NDI-10** and **NDI-6**) in the tested conditions against the bacteria (Table 1). For **NDI-10** in Gram-negative bacteria, the minimal inhibitory concentration (MIC) ranged between 128 μM for *P. aeruginosa* to 8 μM for *E. coli,* while *Klebsiella pneumonia* was altogether resistant. For Gram-positive bacteria, the MIC values were lower in the range than those measured for Gram-negative. The range of activities varied here from MICs of 4 μM for *Enterococcus faecium* strains to 16 μM for *S. aureus* strains (Table 1). **NDI-6** was less active overall when compared to **NDI-10**. Furthermore, Gram-negative bacteria were generally resistant to **NDI-6**, except *A. baumannii* and *Klebsiella aerogenes*, which were found sensitive at high concentrations (64 μM). An MIC that was 4 to 8 times higher than that of **NDI-10** was observed for Gram-positive bacteria (Table 1). On the basis of these data, **NDI-10** was selected for further characterization of the mode of action.

The Gram-Negative Outer Membrane Acts as a Permeability Barrier. The outer membrane of Gram-negative bacteria acts as a permeability barrier hindering the diffusion of antibiotics inside the cells and, therefore, preventing them from reaching their targets.[53] Taking advantage of the **NDI-10** innate fluorescence, we explored its intake for several bacteria, including the resistant strain *K. pneumoniae,* the high/intermediate resistant *A. baumannii,* and the sensitive Gram-negative bacteria *Enterobacter cloacae.* The resistant *K. pneumoniae* was completely impermeable to the drug, while the sensitive *E. cloacae* was quickly stained with the dye in a regular way (just the central part of the bacteria, not

https://doi.org/10.1021/acs.jmedchem.1c01905
J. Med. Chem. 2022, 65, 4752−4766

Table 1. Microorganisms Used in This Work and MIC Values for the Active Compounds[a]

	strains	source	MIC (μM) NDI-10	MIC (μM) NDI-6
Gram-negative	*A. baumannii* LMG 01041	BCCM	64	64
	E. aerogenes LMG 02094	BCCM	32	64
	E. cloacae LMG 02783	BCCM	8	R
	E. coli LMG 8223	BCCM	16	R
	K. pneumoniae LMG 20218	BCCM	R	R
	P. aeruginosa LMG 6395	BCCM	128	R
	S. enterica LMG 07233	BCCM	64	R
Gram-positive	*B. cereus* ATCC 10987	ATCC	8	64
	B. cereus ATCC 14579	ATCC	8	64
	E. faecalis LMG 08222	BCCM	8	64
	E. faecalis LMG 16216	BCCM	4	32
	E. faecalis V583	[51]	4	32
	E. faecium LMG 11423	BCCM	4	16
	E. faecium LMG 16003	BCCM	4	16
	S. aureus LMG 8224	BCCM	16	128
	S. aureus LMG 10147	BCCM	16	128
	S. aureus LMG 15975	BCCM	16	128
	S. epidermidis Tü3298	[52]	16	128

[a]R, resistant to over 128 μM. ATCC, American Type Culture Collection. BCCM, Belgian Coordinated Collections of Micro-organisms.

the poles). The G4-ligand entered *A. baumannii* in a time-dependent manner, which altogether suggests that the outer membrane is acting as a permeability barrier in a strain-specific way (Supporting Information, Figure S1).

To confirm if and determine how the outer membrane affects the activity of **NDI-10**, we tested its activity in the presence of the recently described outer membrane perturbing peptide D-11.[54] As can be seen in Table 2, the antimicrobial activity of **NDI-10** in Gram-negative bacteria was significantly increased by the coincubation with 4 μM of D-11 peptide. This peptide reduced further the **NDI-10** MIC to the range of the Gram-positive bacteria or even lower (0.5−8 μM). Among the bacteria tested, *E. coli* LMG 8223 and *S. enterica* LMG 07233 were the most sensitive strains to the combination, and even *K. pneumoniae* LMG 20218 was sensitized to 16 μM of **NDI-10** after a coincubation with D-11. For the Gram-positive bacteria, no effect on the MIC was observed, as expected (Table 2).

Table 2. MICs for a Selected Gram-Positive and Gram-Negative Bacteria Panel in the Absence or Presence of 4 μM of the Outer Membrane Perturbing Peptide D-11[a]

strains	MIC NDI-10 (μM) +0 μM of D11	+4 μM of D11	MIC_b
A. baumannii LMG 01041	64	8	128
E. aerogenes LMG 02094	32	8	>128
E. cloacae LMG 02783	8	8	8
E. coli LMG 8223	16	<0.5	16
K. pneumoniae LMG 20218	>128	16	>128
P. aeruginosa LMG 6395	128	4	128
S. enterica LMG 07233	64	<0.5	128
B. cereus ATCC 10987	8	8	64
E. faecalis V583	4	4	64
E. faecium LMG 16003	4	4	32
S. aureus LMG 8224	16	16	128

[a]Besides, MIC_b shows the MIC of the bacteria after a first MIC test and bacterial regrowing in a fresh medium to test the bactericidal or bacteriostatic effect of **NDI-10**. A similar MIC value to the first column (+ 0 μM of D11) indicates bactericidal effect, while higher values indicate a bacteriostatic effect.

The Antimicrobial Activity of NDI-10 Is Bacteriostatic or Bactericidal in a Strain-Dependent Manner. The bactericidal/bacteriostatic effect of **NDI-10** was explored. For that, after a first MIC test, the cells were diluted 10 times in a new cationic-adjusted Mueller-Hinton broth (cMHB) medium and grown for another 20 h after a previous MIC test (MIC_b Table 2). The absence of growth at the MIC concentration was considered bactericidal, while the presence of growth indicated a bacteriostatic effect. As seen in Table 2, **NDI-10** was mainly bactericidal for Gram-negative bacteria (except for *E. aerogenes*, which was bacteriostatic), while it was mainly bacteriostatic for Gram-positive bacteria. In this case, the bactericidal MIC was determined at concentrations 8- to16-fold higher than the observed MIC.

To confirm these results, we further explored the effect of **NDI-10** in growing cultures of *E. coli, B. cereus, E. faecium,* and *S. aureus* measuring their optical density at 600 nm (OD_{600}) over time. As seen in Figure 2D, the bacterial growth stopped in a dose-related manner when **NDI-10** was added, as expected for bacteriostatic compounds. To confirm the absence of lytic effects, the cells were prepared at OD_{600} of 0.25 in 4-(2-hydroxyethyl)-1-piperazineethanesulfonic acid with 5% glucose (GHEPES) and incubated for 2 h with different doses of **NDI-10**. The OD_{600} was then measured every 5 min and compared to polymyxin B and gramicidin S (as bacteriolytic controls) and to erythromycin and chloramphenicol (as bacteriostatic controls). As seen in Figure 2E, no OD_{600} alteration was observed for **NDI-10**-treated cells or the bacteriostatic antibiotic controls, while a clear OD_{600} reduction was observed for the bacteriolytic controls. These results suggest that even for *E. coli,* where the activity was bactericidal, no cell lysis was occurring. To check the viability of these cultures and to confirm the bactericidal/bacteriolytic effect after this treatment, we spotted 10 μL in cMHB plates (Figure 2F), and as expected for a bacteriostatic effect, the bacteria could grow again once the compound was eliminated from the medium. For *E. coli,* only a few colonies were observed after 2 h of incubation at the MIC or above the MIC concentrations, which suggests that the bactericidal effect could be time-related for this species.

Transcriptomic Analysis for E. coli and S. aureus Treated with NDI-10. To assess the gene expression effects caused by **NDI-10** and considering the known DNA affinity of the NDIs, a transcriptomic analysis of *E. coli* LMG 8224 and *S. aureus* LMG 8223 as Gram-negative and Gram-positive model organisms, respectively, was performed. The results were then compared with the nontreated controls using the T-REX program[55] (Table 3). Overall and according to the results, *S. aureus* LMG 8224 saw its genomic expression modified in 699 genes out of its 2817 total annotated genes. 335 were upregulated (11.89% of the total genes), and 364 were downregulated (13.92%), adding up to a total of 25% of the modified genomic transcription (Table 3). *E. coli* displayed from its 4930 annotated genes an altered expression in 1527 after a treatment with **NDI-10**. This is 31% of the total genes (Table 3); however, unlike for *S. aureus* (for which a similar number of genes were up- and downregulated), more than 27% of these genes were downregulated, suggesting strong

https://doi.org/10.1021/acs.jmedchem.1c01905
J. Med. Chem. 2022, 65, 4752−4766

Table 3. Functional analysis using gene set enrichment analysis on transcriptomes of *S. aureus* LMG 8224 and *E. coli* LMG 8223 after the treatment with 16 μM of NDI-10[a]

clusters of orthologous groups of proteins (COG)	*S. aureus* LMG 8224					*E. coli* LMG 8223				
	total	up		down		total	up		down	
		No.	%	No.	%		No.	%	No.	%
cell cycle control, cell division, chromosome partitioning	7	1	14.29	2	28.57	26	0	0	16	61.5
cell motility	0	0	0	0	0	34	0	0	1	2.9
cell wall/membrane/envelope biogenesis	33	6	18.18	4	12.12	220	3	1.36	72	32.7
defense mechanisms	20	3	15	2	10	52	0	0	9	17.3
intracellular trafficking, secretion, and vesicular transport	10	2	20	1	10	57	5	8.77	18	31.6
post-translational modification, protein turnover, and chaperones	27	2	7.40	4	14.81	123	2	1.63	52	42.3
signal transduction mechanisms	16	1	6.25	2	12.5	137	0	0	35	25.5
total	113	15	13.27	15	13.27	649	10	1.54	203	31.27
replication, recombination and repair	51	16	31.37	6	11.76	165	7	4.24	28	17.0
transcription	44	8	18.18	7	15.91	263	9	3.42	70	26.6
translation, ribosomal structure and biogenesis	24	2	8.33	3	12.5	89	0	0	45	50.6
total	119	26	21.84	16	13.44	517	16	3.09	143	27.65
amino acid transport and metabolism	83	9	10.84	10	12.05	271	3	1.11	82	30.3
carbohydrate transport and metabolism	49	0	0	9	18.37	312	9	2.88	59	18.9
coenzyme transport and metabolism	36	6	16.67	4	11.11	95	1	1.05	38	40
energy production and conversion	33	6	18.18	3	9.09	250	1	0.40	99	39.6
inorganic ion transport and metabolism	80	13	16.25	11	13.75	236	6	2.54	43	18.2
lipid transport and metabolism	20	0	0	3	15	73	0	0.00	28	38.4
nucleotide transport and metabolism	29	2	6.89	4	13.79	63	1	1.59	17	27.0
secondary metabolites biosynthesis, transport, and catabolism	11	0	0	1	9.09	42	0	0	11	26.2
total	341	36	10.55	45	13.19	1342	21	1.56	377	28.09
function unknown or poorly characterized	119	12	10.08	17	14.28	737	26	3.53	179	24.3
total annotated genes in the genomes	2817	335	11.89	364	12.92	4930	173	3.51	1354	27.5

[a]Total indicates the total of genes described to be associated with the indicated COG categories for each strain. No. shows the number of genes in this COG category up- or downregulated after the **NDI-10** treatment and the % respect the total of the COG categories. Shadowed in white are cellular and signaling-related processes, in light grey are information, storage, and processing-related processes, and in dark grey are metabolism-related processes.

gene repression caused by **NDI-10**, which could be also related to the different bactericidal/bacteriostatic activities observed.

From these genes and based on a Gene Ontology (GO) analysis, 481 genes were identified to be differentially expressed for *S. aureus* when treated with **NDI-10**, while 1291 were found for *E. coli*. These genes can be categorized into 463 functional GO subcategories for the Gram-negative *E. coli* and 215 for the Gram-positive *S. aureus* (http://gseapro.molgenrug.nl/). These subcategories fall into three main groups (https://www.ebi.ac.uk/QuickGO/), which are the biological processes (34.51% and 61.36% of the genes for *E. coli* and *S. aureus*, respectively), cellular components (27.99% and 11.80%), and molecular function (47.56% and 26.80%).

The functions of the assembled genes were further evaluated using a Clusters of Orthologous Groups (COG) analysis in the GSEA-Pro program. Overall, 769 (50.36% of the total) and 153 (21.88%) genes were assigned to 19 and 18 COG categories for *E. coli* and *S. aureus*, respectively (Table 3). *S. aureus* functions related to information, storage, and processing were the most affected by **NDI-10**, with 35.29% of related genes dysregulated, followed by the cellular processes, signaling, and metabolism-related genes with 26.5% and 23.75% of genes dysregulated, respectively. Considering the COG categories, the cell cycle control, cell division, and chromosome partitioning processes were the most downregulated, while those related to replication, recombination, and repair were the most upregulated, indicating a severe stress response (Table 3). For *E. coli*, ∼30% of the genes of the different COG categories were affected (Table 3). Unlike *S. aureus*, the gene repression of **NDI-10** was astonishing and included genes related to critical processes such as translation, ribosomal structure, and biogenesis-related functions, until 50% of these related genes were repressed. Other metabolism-related processes were also strongly repressed, such as enzyme transport and metabolism, energy production and conversion, lipid transport, and metabolism as well as cellular and signaling-related processes, including post-translational modification, protein turnover, and chaperones. Here, up to 40% of the related genes were altered by the G4-ligand used (Table 3).

Relation between the Presence of Putative PQS and Modifications in the Gene Expression. We explored the relationship between the presence of putative G4s and expression levels in genes after treatment with **NDI-10**. As can be seen in Figure 3A,B, the genes with a changed expression were usually found clustered together. This was especially relevant for the downregulated genes of *E. coli* and *S. aureus*, showing that G4 structures can likely be present in promoter regions. In total, 7033 PQS with a high probability of forming (score 40) were identified in *E. coli*. 6764 of them were unique sequences (only repeated once, 92.7%). In *S. aureus* only 154 were found, of which 141 were unique (91.5%; Supporting Information 3 and 4). These data indicate an extraordinary variability in the G4-structures formation, especially in Gram-negative bacteria. Interestingly, 128 sequences found in *S. aureus* (90.7%) were also found in common with *E. coli*, which suggests an important role of these structures in the gene epigenetic control in more complex organisms (Supporting Information 3 and 4).

https://doi.org/10.1021/acs.jmedchem.1c01905
J. Med. Chem. 2022, 65, 4752−4766

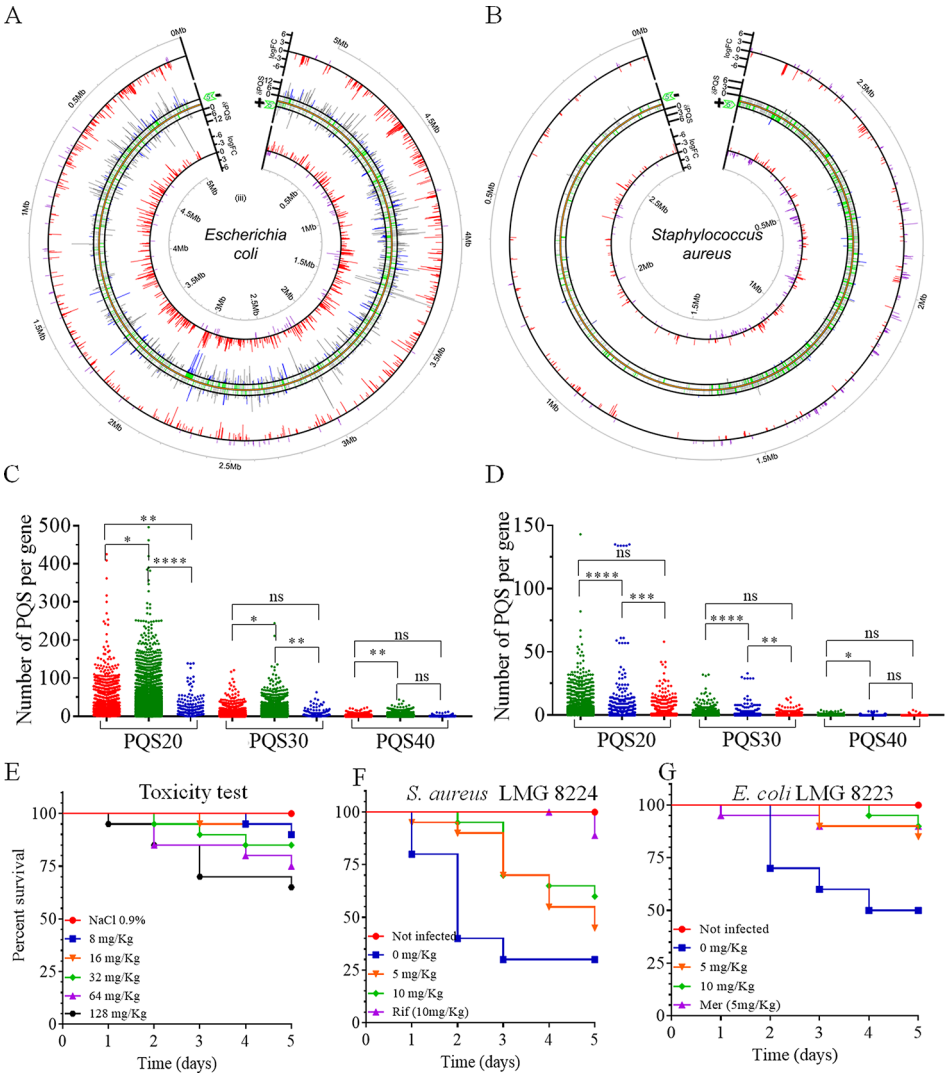

Figure 3. Relation between the expression profile and presence of putative G4 structures (PQS) for *E. coli* LMG 8223 (A) and *S. aureus* LMG 8224 (B). From outside to inside: the size of the genome followed by the expression level of the genes in the sense strand after the treatment with **NDI-10** according to its intensity (log FC from 6 to −9, purple upregulation, red downregulation). Further in, the density of PQS with a high probability of forming a G4 per gene (δPQS40) in the sense strand. In blue, PQS gene density of genes with modified expression levels after treatment, and in gray without expression alterations. The location of the genes in the genome for the sense strand follows, where those in green displayed a changed expression after the treatment, while those in gray did not. Opposite as a mirror image, the location of the genes, PQS densities, and gene expression in the opposite strand are shown. Plots were made with the circlize package.[56] Numbers of PQS for unmodified-expression genes (green), upregulated genes (blue), and downregulated genes (red), while considering three score filters (20/medium, 30/medium-high and 40/high probability of forming a G4) for *E. coli* LMG 8223 (C) and *S. aureus* LMG 8224 (D), respectively, are indicated. Toxicity of **NDI-10** in the *G. mellonella model* (E). Activity of **NDI-10** in *S. aureus* infection model (F) and *E. coli* infection model (G) in *G. mellonella*.

Subsequently, we explored PQS in a broader perspective by considering also another two levels of G4-formation probability (or score), that is, 20 and 30. If we assume that PQSs that score 40 have a high probability of forming a G4, those that score 20 have just a medium probability.[21,38]

As is observable in Figure 3C for *E. coli* LMG 8223, significant differences were observed for the number of PQSs with a medium probability of forming a G4 (PQS20) per up- and downregulated genes (p = 0.0024), but no differences were observed for the other two tested scores. The differences were also significant between the genes without a changed expression after treatment and the up- and downregulated ones at PQS20, (p < 0.0001 and 0.04, respectively) as well as for PQS30 (p = 0.0054 and 0.0126 for up- and downregulated genes, respectively) and PQS40, but only in the case of downregulated genes (p = 0.002). The data suggest that the downregulated genes are more prone to present G4 structures (Figure 3C, NDI sensitives) than the upregulated genes in *E. coli*. In fact, this is the observed tendency, considering the average number of PQS per gene for upregulated or downregulated after the treatment with **NDI-10** (Table 4).

In the Gram-positive *S. aureus,* no significant differences were observed between the number of PQSs at any score. However, and unlike in *E. coli,* the average number of PQSs observed for upregulated genes was higher than for downregulated genes after the treatment with **NDI-10** (Table 4).

These data suggest that G4 could not only be asymmetrically distributed in numbers in Gram-positive and Gram-negative bacteria but also that their role from the point of view of the gene expression control in each bacterial group could be

https://doi.org/10.1021/acs.jmedchem.1c01905
J. Med. Chem. 2022, 65, 4752−4766

Table 4. Average PQS Per Gene Considering Three Different PQS Scores[a]

	PQS score	transcription	*E. coli*LMG 8224	*S. aureus*LMG 8223
average number of PQS per gene ± SE	20	down	37.5 ± 1.1	5.0 ± 0.1
		unmodified	42.7 ± 0.8	5.0 ± 0.2
		up	27.5 ± 2.4	8.7 ± 1.0
	30	down	8.7 ± 0.3	0.9 ± 0.0
		unmodified	10.5 ± 0.3	0.9 ± 0.0
		up	7.2 ± 0.9	1.6 ± 0.2
	40	down	1.0 ± 0.0	0.05 ± 0.0
		unmodified	1.4 ± 0.1	0.05 ± 0.0
		up	0.9 ± 0.1	0.10 ± 0.0

[a]Down, up, and unmodified shows the changes in the gene transcription.

different. Finally, it must be noted that several genes with putative PQSs were unmodified in their expression after the **NDI-10** treatment. This could be related to specificities between G4s ligands and G4 structures or false prediction of G4s.

Biophysical Assay of Six Selected PQSs of E. coli and S. aureus. To verify the effective interaction and stabilization of G-quadruplex structures of *E. coli* and *S. aureus* genome by **NDI-10**, we selected six PQSs (Supporting Information, Table S1) according to the higher score previously obtained with G4-iM Grinder. Their propensity in G4-folding was confirmed by circular dichroism (CD) spectra recording in 10 mM lithium cacodylate buffer (pH 7.4) in the presence of 100 mM potassium chloride (Supporting Information, Figure S2). In particular, SA-3 can fold into a "hybrid" 3 + 1 G4-topology (maxima at 295 and 265 nm; minimum at 242 nm); SA-5, EC-6, and EC-9 present a predominant parallel G4 topology (maximum at ∼264 nm and a minimum at ∼240 nm); SA-7 and EC-6 spectra correspond to a mix of parallel and antiparallel G4-topology conformations, with a mainly antiparallel component for SA-7 (maximum at 295 nm) and a parallel one for EC-6 (maximum at 262 nm).[57]

To properly define the G4-ligands contribution in thermal stabilization of these new identified G4s, potassium concentrations were chosen to reach a melting temperature of the oligonucleotide alone at ∼50−70 °C. The ability in the G4-folding of these PQSs was also verified in the presence of the lower potassium concentrations used (Supporting Information, Figure S3).

The ability in stabilizing these G4 sequences was tested for all the 14 NDI compounds by FRET-melting (FRET = Förster resonant energy transfer),[58] highlighting the high binding ability of **NDI-10** above all other G4-ligands (Supporting Information, Table S2). Despite the melting temperature (Tm) identified for PQSs alone ranging between 50 and 55 °C, **NDI-10** binds these structures so strongly that it is not possible to define a value of Tm in its presence. Indeed, Tm values in the presence of **NDI-10** resulted over the temperature of 95 °C for all sequences except SA-3, which in any case is stabilized by over 34 °C. Among all the tested G4-ligands, also **NDI-8** strongly stabilized the PQSs, as expected from its high electrostatic interaction ability due to its positive charge. Nevertheless, although it is an excellent binder from a biophysical point of view, no antimicrobial activity was observed. This result suggests that other factors as membrane permeability to the compounds also play an important role in the sensitivity. In this case, we speculate that the very high net positive charge can increase the difficulty for it to cross the negatively charged bacterial membranes (could be retained in membranes), reducing the drug permeability and the ability to reach DNA. In fact, and in the case of NDI-10, the membrane permeability has been related to antimicrobial activity (Supporting Information, Figure S1).

To gain a deeper and more precise analysis of G4-stabilizing ability, we performed CD-melting experiments in the presence of **NDI-6** and **NDI-10**, which both show antimicrobial activity. The strong binding interaction of **NDI-10** toward selected PQSs was confirmed also by CD values, whose stabilization range goes from 18.8 °C in the case of EC-9 until greater than 35.6 °C in the case of SA-7 (Table 5). **NDI-6** is also able to stabilize the tested sequences, albeit to a much lesser extent, with an average degree of stabilization of ∼15 °C.

Hemolytic Activity, In Vivo Toxicity, and Antimicrobial Activity in Galleria mellonella. Despite the fact that toxicity close to the MIC has been previously described for **NDI-10** in eukaryotic immortalized cell lines,[62] no hemolytic activity was observed after the exposition of human purified erythrocytes at concentrations between 1 and 128 μM. Next, to get insight into possible toxicity and in vivo activity, we tested the toxicity and activity of **NDI-10** in a *Galleria mellonella* infection model. This assay is considered a "non-animal model", but it allows the evaluation of active compounds in more complex environments similar to the expected effects in mammals and with the presence of an innate immune system. The ability to use large groups of subjects and the simple maintenance and manipulation of the worms makes the model

Table 5. CD-Melting Result[a]

		PQSs alone	NDI-10		NDI-6	
PQSs	$[K^+]$ (mM)	Tm (°C)	Tm (°C)	ΔTm (°C)	Tm (°C)	ΔTm (°C)
SA-3	20	61.0 ± 0.3	88.3 ± 0.2	24.5	77.6 ± 0.4	16.6
SA-5	5	64.2 ± 0.9	>95	>30.8	76.2 ± 0.9	12
SA-7	100	59.4 ± 0.2	>95	>35.6	74.3 ± 0.2	14.9
EC-6	0.5	60.0 ± 0.3	91 ± 1	31	72.2 ± 0.5	12.2
EC-7	0.5	70.2 ± 0.6	>95	>24.8	92.8 ± 0.7	22.8
EC-9	5	63.7 ± 0.8	82.5 ± 0.9	18.8	78 ± 1	14.3

[a]ΔTm values measured by CD melting of 2.5 μM oligonucleotides, in the presence of 10 μM G4-ligands (4 equiv), in 10 mM lithium cacodylate buffer (pH 7.4), at the indicated K^+ concentrations. The ellipticity changes were recorded at the maximum wavelength (290 nm for SA-7, 260 nm for all the other G4-sequences).

https://doi.org/10.1021/acs.jmedchem.1c01905
J. Med. Chem. 2022, 65, 4752−4766

very useful to study the pathogenicity, the pharmacokinetics, and the toxicity of these antibiotics.[59−61] Thus, the model was considered for a preliminary test of the putative toxicity of **NDI-10** and its activity in vivo in infection models with *E. coli* and *S. aureus*. As can be seen in Figure 3E, no apparent acute toxicity was observed for **NDI-10**. The median lethal dose (LD50) was not reached even at the highest dosage administered after 5 d (128 mg/kg; 65% of survival). Interestingly, the compound was detected in the worm feces after the administration, which suggests that it is being processed and eliminated. The nonaccumulation of the drug in the worms is possibly related to the high tolerance displayed, suggesting that NDI-10 can potentially be safe at concentrations higher than the determined MIC in living organisms. Despite this encouraging finding, future research will be focused on reducing possible toxicity in eukaryotic (noncancer) cell lines, increasing the specificity toward bacteria, to increase the in vivo applicability of these compounds.

In the infection model with *S. aureus* (Figure 3F) when treated with 5 or 10 mg/kg of **NDI-10**, the mortality of the worms was reduced in comparison to the untreated control. Interestingly, after 3 d, only 30% of the untreated worms survived in comparison to 70% of the treated worms. In the case of *E. coli*, a protective effect was also observed. At the end of the treatment, 90% of the worms survived the infection, while only 50% survived the infection alone (Figure 3G). The differences observed between the two models can be related to the different mechanisms of action of the compound in each bacterial species as well as the elimination of the drug by the worms. For *S. aureus,* **NDI-10** displayed bacteriostatic properties that can be related to a less effective and time-dependent effect. On the contrary, for *E. coli* the effect was bactericidal, and the total eradication of the bacteria was probably responsible for the better survival from the infection after 5 d.

CONCLUSIONS

Here, we have tested the possibility of using G4-DNA domains as targets to treat bacterial infections by employing known G4-ligands. Interestingly, our data suggest that some NDIs can effectively inhibit or kill bacteria at similar concentrations as current antibiotics. The Gram-positive bacteria analyzed here were characterized by the presence of a lower number of putative G4 domains than in Gram-negative bacteria and a higher sensitivity to the **NDI-10**, the more active tested NDIs. In the case of Gram-negative bacteria, the presence of the outer membrane protected from the effect of **NDI-10** in a species-dependent manner, as the combination with the outer-membrane perturbing peptide D-11 showed. Notably, and despite the high resistance, the drug was mainly bactericidal for Gram-negative bacteria, while it was bacteriostatic for Gram-positive bacteria. No lysis of the cells was observed in Gram-negative or -positive bacteria, which suggests that the action mechanism of this drug is likely related to the inhibition of critical processes associated with gene transcription or protein translation. In fact, a different gene expression profile was observed for the Gram-positive bacteria *S. aureus* and the Gram-negative *E. coli.* Although the in silico analysis showed that the putative number of G4s in *S. aureus* was much lower than for *E. coli*, the number of genes with altered expression after the treatment with **NDI-10** was similar for both bacteria (25% and 30% of the total annotated genes, respectively). However, the number of upregulated genes and downregulated genes in *S. aureus* was similar, while for *E. coli* a strong gene repression was observed. These data suggest a better adaptive response for Gram-positive bacteria than for Gram-negative, which could be related to the different bacteriocidal effects of the compound. In addition, some preliminary biophysical studies on model oligonucleotides supported the thesis that the antimicrobial activity of **NDI-10** is directly correlated to the G4-bind and stabilization ability. Besides, it must be added that the data suggest that the role of G4 could be different in Gram-positive and Gram-negative bacteria, since the average PQS numbers are higher in downregulated genes than upregulated ones in *E. coli*, and the opposite is seen in *S. aureus*. This different mode of action was also observed in the *G. mellonella* infection model used. A better protective effect was observed against *E. coli* than against S. *aureus*, which could be related to the ability of the worm to excrete the drug. This drug excretion is probably also related to the low toxicity levels observed.

Overall, our results suggest that DNA G4s can be used as new targets in bacteria, and the design of new and potent G4 ligands can be a good option in the design and development of new antimicrobials. However, a large optimization to increase the selectivity and activity toward bacteria is still necessary.

EXPERIMENTAL SECTION

Microorganisms and Growth Conditions. The bacterial strains used in this study are listed in Table 1. Gram-negative bacteria were grown as standing cultures at 37 °C and shaking (200 rpm) in Luria−Bertani broth medium (LB, Sigma-Aldrich). Gram-positive bacteria were statically grown at 37 °C in M17 broth (Difco BD) supplemented with glucose at a concentration of 0.5% (w/w). For solid media, agar at 1.2% was added.

In Silico Analysis with G4-iM Grinder. In this work, we used G4-iM Grinder to analyze the prevalence and importance of quadruplex structures in the genome of all bacteria.[38] G4-iM Grinder is an R-based algorithm that locates, quantifies, and qualifies PQS, PiMS, and their potential higher-order versions in RNA and DNA in genomes. 1222 raw fasta sequences of the bacteria were retrieved from the NCBI database[63] (Supporting Information 1). As a workflow, we applied the functions *G4iMGrinder* (to find quadruplex candidates) and *G4.ListAnalysis* (to analyze the results per genome) from the G4-iM Grinder package (GiG) on all the bacterial genomes. The quadruplex definitions were left as the predefined setup of the package for the initial exploratory analysis on the 1222 bacterial genomes. The "size-restricted overlapping search and frequency count" method (Method 2, M2A and M2B) filter was used to locate all the potential candidates. Then these PQSs were evaluated by their probability of quadruplex-formation score (as the mean of G4Hunter[64] and PQSfinder algorithms[65]), their frequency of appearance in their genome, and the presence of known-to-form quadruplex structures within. The G4-iM Grinder database, which includes over 2800 sequences related to G4 and i-Motifs, was used to find these matches (ver. 2.5).

To compare the potential quadruplex presence and prevalence between genomic groups, we calculated the genomic density of several subjects. The density of counts was used instead of the total number of counts to compare efficiently between different size genomes (density = number of results per 100 000 nucleotides). These values were obtained using the *GiGList.Analysis* function of the G4-iM Grinder package. The arguments for the analysis were (1) the density of results (PQS) with score filters (score ≥ 40; sequences with a HIGH probability of forming a G4) and (2) density of PQS with known G4 within their sequence.

The search for PQS was repeated for the genomes of the bacteria tested in vitro and in vivo, *S. aureus* (RefSeq ATCC_25923_ASM75620v1), and *E. coli* (RefSeq ATCC_25922_ASM74325v1). For this extensive search, the parameters introduced to the algorithm were broadened to allow the detection of

https://doi.org/10.1021/acs.jmedchem.1c01905
J. Med. Chem. 2022, 65, 4752−4766

2-sized G-runs and longer loops (MinRunSize = 2, MaxLoopSize = 30, MaxPQSSize = 50, and MaxIL = 2 (max number of bulges in total)). Although sequences with these characteristics can form G4s,[12,66] they are expected to have a lower stability. Hence, the results were filtered by their probability of forming a G4. The candidates with a high probability of forming a G4 (Score ≥ 40), with medium-high probability (Score ≥ 30), and medium probability (Score ≥ 20) were considered and investigated for the posterior studies with the transcriptomic results.

NDIs Derivatives Synthesis and Purification. All the solvents and reagents for the chemical synthesis were purchased from Alfa Aesar, Merck, and TCI and were used without further purification. A high-performance liquid chromatography (HPLC) analysis was performed using an Agilent system SERIES 1260 with a Waters XSelectHSSS C18 column (2.5 μm, 4.6 × 50 mm). The following method was used: flow 1.4 mL/min, isocratic gradient over 2 min with 95% of H_2O and 0.1% trifluoroacetic acid (TFA) (5% CH_3CN), gradually to 40% aqueous solvent over 6 min, then an isocratic flow for 4 min (λ = 256 nm). All the compounds tested were used with a purity greater than 95%, as confirmed by HPLC profiles reported in the Supporting Information file.

HPLC purifications were performed by an Agilent Technologies 1260 Infinity preparative HPLC provided with a diode array UV−vis detector. The column was a Waters XSelect CSH Phenyl-Hexyl 5 μm (150 × 30 mm), and the flow was 30 mL/min. Purification Method A: isocratic flow over 2 min with 95% of aqueous solution (0.1% trifluoroacetic acid in milli-Q water) and 5% organic solvent (acetonitrile), gradually to 60−40%, respectively, over 14 min (λ = 280, 500 nm).

^{1}H NMR and ^{13}C NMR spectra were recorded on a Bruker Avance 300 MHz spectrometer. High-resolution mass spectrometry (HRMS) spectra were recorded on a UHPLC-HRMS/MS-AB Sciex X500B spectrometer. The synthesis and characterization of **NDIs 1−6**,[37,45] **NDI-8**,[46] and **NDI-10−14**[31,32,47,48] have been reported in previous works. Analytical HPLC profiles and NMR characterizations resulted in results that were comparable with those available in the literature, confirming the identity and purity of the compounds.

Synthesis of **NDI-7**: 430 mg (0.726 mmol) of synthetic **NDI-15**[49] and 4 equiv of 1-aminopropane (2.90 mmol, 240 μL) were dissolved in 70 mL of CH_3CN and refluxed for 1 h. The crude was checked by analytical HPLC, getting the desired product **NDI-16** in a mixture with the relative dehalogenated compound **NDI-6** (Figure 2C, step a). The solvent was evaporated under vacuum, and the red solid was resuspended in saturated solutions of $NaHCO_3$ and extracted by dichloromethane. The solvent of the resulting organic phase was evaporated, and the crude extract was used for the following step. 300 mg of the mixture was suspended in neat 1-aminopropane (1 mL) in a sealed vessel (Figure 2C, step b). The microwave-assisted reaction was performed at 150 °C for 10 min under stirring (250 psi). After the reaction mixture was cooled to room temperature, an acidic aqueous solution (HCl 10%) was added, and the resulting blue mixture was purified by preparative HPLC (Method A previously reported).

NDI-7 was obtained as a blue solid with a 63% yield (analytic HPLC rT = 6.34 min; purity 100%) (Supporting Information).

NDI-7. ^{1}H NMR (300 MHz, D_2O): 7.41 (s, 2H$^+$), 4.05 (t, J = 6.7 Hz, 4H$^+$), 3.31 (t, J = 7.0 Hz, 8H$^+$), 2.98 (s, 12H$^+$), 2.15−2.11 (m, 4H$^+$), 1.89−1.82 (m, 4H$^+$), 1.18 (t, J = 7.3 Hz, 46$^+$). ^{13}C NMR (75 MHz, D_2O): 164.9, 162.7, 148.3, 123.7, 119.4, 118.1, 117.0, 99.8, 55.0, 44.4, 42.6, 37.3, 22.8, 21.9, 10.9. HRMS Calcd for $C_{30}H_{42}N_6O_4$, [M + H]+: 551.3340 Da, found 551.3315 Da (Supporting Information).

Synthesis of **NDI-9**: 229 mg (0.385 mmol) of synthetic **NDI-15**[49] and 3 equiv of piperidine (1.156 mmol, 114 μL) were dissolved in 70 mL of CH_3CN and refluxed for 2 h (Figure 2C, step c). The solvent was removed under vacuum, and the solid mixture was purified by preparative HPLC (Method A previously reported). **NDI-9** was obtained as a purple solid with a 68% yield (analytic HPLC rT = 5.47 min; purity 99.1%) (Supporting Information).

NDI-9. ^{1}H NMR (300 MHz, D_2O): 8.16−8.11 (m, 2H$^+$); 7.91 (d, J = 7.9 Hz, 1H$^+$); 4.12−4.03 (m, 4H$^+$); 3.42 (bs, 4H$^+$); 3.25−3.19 (m, 4H$^+$); 2.87 (s, 12H$^+$); 2.06−2.07 (m, 4H$^+$); 1.72 (bs, 6H$^+$). ^{13}C NMR (75 MHz, D_2O): 164.0, 163.6, 161.8, 153.7, 130.1, 129.8, 126.6, 125.1, 124.6, 123.0, 119.8, 114.3, 104.1, 55.3, 55.1, 53.7, 42.7, 37.5, 26.0, 22.9, 22.7. HRMS Calcd for $C_{29}H_{37}N_5O_4$, [M + H]+: 520.2918 Da, found 520.2899 Da (Supporting Information).

Antimicrobial Susceptibility Test. NDI conjugates were resuspended in DMSO (Sigma-Aldrich) at 10 mM. The minimal concentration inhibition test was performed by the broth microdilution method in 96-well plates at concentrations ranging from 128 to 2 μM according to CLSI guidelines in cMHB (Difco BD).[50] Briefly, the 96-well plates were filled with 50 μl of culture medium, and the compounds were twofold serially diluted at 2-times the desired concetration. The indicator strains were cultured for 20 h in agar plates at 37 °C. A few colonies were streaked from the plate and resuspended in NaCl 0.9% to prepare a 0.5 McFarland scale cell suspension (∼1.5 × 10^8 CFU/mL). The bacterial inoculum was prepared in cMHB at 5 × 10^5, and 50 μL of this suspension was added into 96-well previously prepared plates to make the final volume 100 μL. The plates were incubated at 37 °C for 20 h, and the growth inhibition was assessed by measuring the OD_{600} using a microplate reader (Tecan Infinity F200). The lowest concentration of antimicrobials that inhibits the visible growth of the indicator strain is identified as the MIC value. The tests were performed in triplicate.

Gram-Negative Outer Membrane Permeability Test. The outer membrane in Gram-negative bacteria acts as a permeability barrier for several antibiotics. Taking advantage of **NDI-10** being fluorescent in the red channel we explored the ability to enter inside the cells using a time-lapse microscope (Delta Vision IX7I microscope, Olympus) equipped with a temperature-controlled system (cube and box incubation system, Life Imaging Services) in similar conditions to those described by Hernandez-Valdes et al., 2020.[67] Briefly, a standard microscope slide was prepared with a 65 μL Gene Frame AB-0577 (1.5 × 1.6 cm) (Thermo Fisher). After that, a chemically defined medium[68] plus 0.5% (w/v) of glucose was prepared and melted with 1.5% (w/v) of high-resolution agarose (Sigma-Aldrich). Thirty microliters of the medium was disposed of in the middle of the frame and covered with another microscope slide to create a homogeneous thin layer of the chemically defined medium. On another side, three Gram-negative bacteria with different resistance levels to the compound as *K. pneumoniae* LMG20218, *A. baumannii* LMG 01041, and *E. cloacae* LMG 02783 were grown for 18 h in LB and washed three times in NaCl 0.9% and prepared at OD_{600} of 0.5. At 0.5X the MIC of **NDI-10** was added (64, 32, and 4 μM, respectively), and quickly 1 μL was spotted on the agar medium. The frame was sealed with a standard microscope coverslip and introduced into the microscope. Microscopy observations and time-lapse recording were performed at 37 °C for 6 h. Images were obtained with a CoolSNAP HQ2 camera (Princeton Instruments) at 100× magnification. Snapshots were collected at the bright-field and red channel (587/610 nm excitation/emission) every 1 h for 6 h and analyzed using ImageJ software.[69]

For outer membrane permeabilization assays, **NDI-10** was tested at concentrations ranging between 32 and 0.5 μM against Gram-negative bacteria (and selected Gram-positive bacteria as a control) in the presence of the outer membrane disrupting peptide L-11[54] at 4 μM. The test was performed in triplicate in the same condition as described before for the MIC test.

Action Mechanism Determination. To explore whether the antimicrobial effect of **NDI-10** was bacteriostatic (inhibition of the bacterial growth) or bactericidal (bacteria eradication), a regular MIC test was performed as described above at concentrations ranging between 128 and 2 μM in 96-wells plates and incubated for 20 h at 37 °C. Then the OD_{600} for this plate was recorded in a Tecan Infinity F200, and each of the wells was used as an inoculum (at 10%) in a newly prepared 96-well plate just with cMHB (no antimicrobial). These plates were incubated for 20 h at 37 °C, and the OD_{600} was monitored at the end in a Tecan Infinity F200. The absence of growth at the same concentration in both assays was considered as a

https://doi.org/10.1021/acs.jmedchem.1c01905
J. Med. Chem. 2022, 65, 4752−4766

bactericidal effect, while the presence of growth at concentrations higher than the MIC was reported as a bacteriostatic effect. The test was performed in triplicate.

The effect on actively growing cultures was also analyzed. For that, the four selected bacteria (*E. coli* LMG 8223, *B. cereus* ATCC 10987, *E. faecium* LMG 16003, and *S. aureus* LMG 8224) were inoculated at 2% in a 96-well plate and incubated at 37 °C in a Tecan Infinity F200, with the OD_{600} being monitored every 5 min during 8 h. When the exponential phase was started (~3 h after the start point) **NDI-10** at different concentrations (32, 16, 8, and 4 μM for *E. coli* and 16, 8, 4, and 24 μM for the Gram-positive bacteria) was added, and the evolution of the growth was monitored until 8 h.

To analyze if **NDI-10** displays a lytic effect or not, a selected group of bacteria (as before) was grown for 20 h, and after that, the cells were washed three times in 4-(2-hydroxyethyl)-1-piperazineethanesulfonic acid (HEPES) buffer (Sigma-Aldrich) with 5% glucose and adjusted to an OD_{600} of 0.5 in the same buffer. After that, the cells were exposed to **NDI-10** in the same conditions as before, incubated at 37 °C, and the decrease in the OD_{600} was monitored every 15 min for 2 h. Polymyxin at 2 μM and erythromycin at 32 μM were used as lysis positive and negative controls for bacteriolysis and bacteriostatic effect in the case of *E. coli*, while gramicidin S at 2 μM (bacteriolytic) and chloramphenicol at 16 μM (bacteriostatic) were used for the Gram-positive strains. After the incubation time of this assay, the cells were centrifuged and resuspended in a HEPES buffer. Ten microliters of each treatment was spotted on a cMHB solid medium and incubated at 37 °C for 20 h. The absence of growth was related to the bactericidal effect. The test was performed in triplicate.

RNA Isolation. For the RNA isolation, *E. coli* LMG 8223 and *S. aureus* LMG 8224 were grown for 20 h in a cMHB medium at 37 °C with shaking (200 rpm). The next day, 10 mL of new cMHB was inoculated at 55 with these cultures and incubated in the same conditions until the OD_{600} value was 1. At this point, 16 μM of **NDI-10** was added, and the cells were incubated for 1 h more. Finally, the cells were collected and washed three times in NaCl 0.9%, removing as much buffer as possible at the end. Cell pellets were resuspended in 400 μL of TE buffer (Tris 10 mM, EDTA 1mM, pH:8) and transferred to screw-cap tubes containing 0.5 g of glass beads, 50 μL of 10% sodium dodecyl sulfate (SDS) (Sigma-Aldrich), and 50 μL of acid-phenol/chloroform/isoamyl alcohol (125:24:1 v/v, Thermo Fisher) pH 4.5. The mixes were placed in a bead beater, and two 1 min pulses at 4 °C were applied to disrupt the cells. The tubes were centrifuged at 14.000 rpm for 10 min at 4 °C, and the upper phase was transferred to a new tube with 500 μL of chloroform/isoamyl alcohol (24:1 v/v). The samples were mixed and centrifuged in the same conditions. The upper phase was used for RNA purification using the Roche High Pure RNA isolation kit (Roche) according to the supplier's recommendations. The different reagents and buffers used were RNA-grade. The solutions were treated with diethyl pyrocarbonate (DEPC, Sigma-Aldrich) in the proportion 1:1000 (v/v), incubated for 20 h at 37 °C, and autoclaved. The RNA quality was electrophoretically evaluated following the "bleach gel" method,[70] and the concentration was measured in a NanoPhotometer N60 (IMPLEN).

Transcriptomic and Data Analysis. The Zymo-Seq RiboFree Total RNA Library Kit (Zymo Research) was used to prepare the library preps for Illumina sequencing using 800 ng of the extracted total RNA. Samples were sequenced on the Illumina NexSeq 500 to generate 75 bases single-end reads (75SE) with an average read depth of 12 M reads per sample. The quality of the resulting fastq reads was checked using FastQC v0.11.9 (Babraham Bioinformatics) and mapped on the reference genome using Bowtie2 v2.4.2[71] using default settings. The resulting SAM files were converted to BAM using SAMtools 1.11,[72] and featuresCounts 2.0.1[73] was used to get the gene counts. The T-REx Web server[55] was used to perform the statistical analysis and determine differential gene expressions (DGE), and subsequently, a gene set enrichment analysis was done for a functional analysis using the GSEA-Pro web server (http://gseapro.molgenrug.nl).

Biophysical Studies. To record CD spectra, all commercial oligonucleotides were diluted from stocks to a final concentration of 2.5 μM in 10 mM lithium cacodylate buffer (pH 7.4) containing 100 mM KCl. The solutions were annealed with heat at 95 °C for 5 min and gradually cooled to room temperature for 4 h. CD spectra were recorded on the Jasco model J-1500 spectropolarimeter (JASCO Corporation), equipped with a Peltier temperature controller, at 25 °C and using a quartz cell of 1 mm optical length, an instrument scanning speed of 50 nm/min with a response time of 2 s over a wavelength range of 215−340 nm with a 1 nm sampling interval. The reported spectra of each sample represent the average of three scans and are baseline-corrected for signal contributions due to the buffer mixture. Observed ellipticities (in millidegrees) were converted into Molecular Ellipticity considering sample concentrations, cuvette path length, and the number of nucleobases that composed the oligonucleotides analyzed. For the CD-melting experiments of G4 structures, the oligonucleotides were annealed in the same way previously reported, dissolving 2.5 μM in 10 mM lithium cacodylate buffer (pH 7.4) in the presence of different KCl concentrations to maintain the initial melting temperature (Tm) values in the 60−70 °C range (Supporting Information, Table S2). To evaluate the G4-ligands contribution, 4 equiv of **NDI-6** and **NDI-10** (10 μM) was added to the mixture and left to equilibrate for 16 h at 20 °C. The ellipticity changes were recorded at the maximum wavelength (290 nm for SA-7, 260 nm for all the other G4 sequences) every 0.1 °C with a temperature scan rate of 5 °C/min in the range of 20−95 °C. Melting temperature (Tm) values were identified according to the van't Hoff equation applied for a two-state transition from a folded to unfolded state, assuming that the heat capacity of the folded and unfolded states are equal.[74]

FRET-melting experiments were recorded by an AriaMx Real-Time PCR System (Agilent Technologies) using *FAM* (6-carboxyfluorescein) 5′-end- and *Tamra* (6-carboxy-tetramethylrhodamine) 3′-end-labeled oligonucleotides.[58] In a total volume of 20 μL, 0.25 μM of tagged oligonucleotides was dissolved in a 10 mM lithium cacodylate buffer at pH 7.4 in the presence of different potassium chloride concentrations according to CD data and to maintain the initial melting temperature (Tm) values in the 50−55 °C range (Supporting Information, Table S2). The mixtures were then annealed by heating at 95 °C for 5 min and gradually cooled to room temperature over 4 h. Subsequently, 4 equiv of each G4-ligands (1 μM) was added and left to equilibrate over 16 h at 20 °C before fluorescence melting curves were recorded. After a first equilibration step at 25 °C for 5 min, a stepwise increase of 5 °C/min was performed to reach 95 °C, the fluorescence emission being measured at 516 nm (excitation at 462 nm) according to an SYBR/FAM optical cartridge (Agilent). The final analysis of the data was performed using OriginPro 8.5 software. Tm values were the average of three experiments, and ΔTm was calculated as the difference of Tm in the presence and absence of the compounds.

Hemolytic Activity and In Vivo Toxicity and Activity in the Galleria mellonella Model. A toxicity analysis was performed with the worms in the sixth developmental stage of the greater wax moth *G. mellonella* according to previously described protocols.[59,75] Three batches of larvae were obtained from a local supplier (Frits Kuipers) combined, and stored in the dark at 20 °C with wood shavings before use. Larvae with ~0.25 ± 0.5 were used in the experiment. For each treatment, 20 healthy worms were placed in Petri dishes, and 10 μL of the compound was injected into the larvae hemocoel through the last left proleg, using 30 G needles and a 500 μL Hamilton repeating dispenser. The final dosages injected into the worms were 8, 16, 32, 64, and 128 mg/kg. NaCl 0.9% was used as a negative control. The inoculated lavages were incubated at 37 °C for 5 d reporting mortality daily.

An in vivo activity test was also performed considering this model and following previously described methodologies with minor changes.[76,77] For that, *G. mellonella* was infected with *E. coli* LMG 8223 and *S. aureus* LMG 8224. Briefly, the bacterial cells were washed three times in NaCl 0.9% and diluted to an OD equivalent to 0.5 McFarland scale (1.5×10^8 CFU/mL). After those six, decimally

https://doi.org/10.1021/acs.jmedchem.1c01905
J. Med. Chem. 2022, 65, 4752−4766

serial dilutions were performed for the bacteria, and 10 μL of each dilution were injected as described above to identify the lethal dosage for each strain. It is desirable to have a concentration of bacteria that is not able to kill the worm quickly. Once the infective dosage was optimized for each bacteria, groups of 20 worms were infected by the injection of 10 μL of the appropriate bacteria dosage (10^5 CFU/worm for *S. aureus* and 10^6 CFU/worm for *E. coli*) in the left proleg. NaCl 0.9% was used in the negative control (no infected worms, just to evaluate the damage of the injection). The infected worms were incubated for 1 h at 37 °C, and after that, they were treated with **NDI-10** at dosages of 5 and 10 mg/kg of **NDI-10**, Meropenem at 5 mg/kg (positive control for *E. coli*), rifampicin at 10 mg/kg (positive control for *S. aureus*), or NaCl 0.9% as the negative control. The injection was performed in the last right proleg, the worms were incubated at 37 °C, and the mortality was monitored for 5 d.

For the hemolytic activity of NDI-10, human blood of healthy individuals was obtained from Sanquin (certified Dutch organization responsible for meeting the need in healthcare for blood and blood products, https://www.sanquin.nl/). For the erythrocyte isolations, 10 mL of blood was centrifuged at 1000*g* for 10 min, and the yellow supernatant was removed. The pelleted cells were washed five times with a NaCl 0.9% solution (raising to 10 mL each time) in the same conditions and finally resuspended in the same volume of buffer (10 mL). In a 96-well plate, the **NDI-10** was added in a volume of 40 μL of NaCl 0.9%, and 160 μL of 10-fold diluted red cells was added to get a final concentration of the compounds ranging between 128 and 1 μM. Triton X-100 at 1% was used as a positive lysis control. The mix was incubated at 37 °C for 1 h, and after that, the samples were centrifuged (1000*g* for 10 min) to remove the intact erythrocytes, and the supernatant was transferred to a new 96-well plate. The release of hemoglobin absorbance was measured at OD_{540}, and the percentage of hemolysis was calculated as $[(HA - H0)/(H^+ - H0)] \times 100$, where HA was the absorbance at OD_{540} of the samples, H0 for the negative control, and H^+ for the positive control.

Statistical Analysis. A statistical analysis and figures design were performed using Graph-Pad Prism 7. A one-way analysis of variance (ANOVA) with the no-parametric test Kruskal–Wallis to compare groups was used to calculate *p*-values (*$p < 0.05$, **, $p < 0.01$; ***, $p < 0.001$; ****, $p < 0.0001$; ns, not significant) and the means ± standard error.

■ ASSOCIATED CONTENT

Supporting Information

The Supporting Information is available free of charge at https://pubs.acs.org/doi/10.1021/acs.jmedchem.1c01905.

Time-lapse microscopy for NDI-10 intake of three Gram-negative strains according to their sensitivity. CD spectra of new G-quadruplex structures at 100 mM KCl concentration. CD spectra of new G-quadruplex structures at different KCl concentrations. Model oligonucleotides used for biophysical studies. FRET-melting results. HPLC purity analysis, ^1H & ^{13}C NMR data, HMRS mass spectra of the tested compounds (PDF)

List of genomes used for the in silico analysis for the presence of G4s (XLSX)

Identified and characterized G4 sequences in Gram-positive and Gram-negative bacteria (XLSX)

δPQS and sequences identified in the genome of *E. coli* LMG 8223 (XLSX)

δPQS and sequences identified in the genome of *S. aureus* LMG 8224 (XLSX)

NDIs molecular formula strings (SMILES) (CSV)

Accession Codes

The transcriptome (RNA sequencing) data that support the findings of this study have been deposited in the NCBI Sequence Read Archive (SRA) with the accession code GSE178890.

■ AUTHOR INFORMATION

Corresponding Authors

Oscar P. Kuipers − *Department of Molecular Genetics, Groningen Biomolecular Sciences and Biotechnology Institute, University of Groningen, 9747AG Groningen, The Netherlands*; orcid.org/0000-0001-5596-7735; Email: o.p.kuipers@rug.nl

Filippo Doria − *Department of Chemistry, University of Pavia, I-27100 Pavia, Italy*; Email: filippo.doria@unipv.it

Rubén Cebrián − *Department of Molecular Genetics, Groningen Biomolecular Sciences and Biotechnology Institute, University of Groningen, 9747AG Groningen, The Netherlands*; Email: r.cebrian.castillo@rug.nl

Authors

Efres Belmonte-Reche − *Advanced (magnetic) Theranostic Nanostructures Lab, International Iberian Nanotechnology Laboratory, 4715-310 Braga, Portugal*

Valentina Pirota − *Department of Chemistry, University of Pavia, I-27100 Pavia, Italy*

Anne de Jong − *Department of Molecular Genetics, Groningen Biomolecular Sciences and Biotechnology Institute, University of Groningen, 9747AG Groningen, The Netherlands*

Juan Carlos Morales − *Department of Biochemistry and Molecular Pharmacology, Instituto de Parasitología y Biomedicina, CSIC, 18016 Granada, Spain*

Mauro Freccero − *Department of Chemistry, University of Pavia, I-27100 Pavia, Italy*; orcid.org/0000-0002-7438-1526

Complete contact information is available at: https://pubs.acs.org/10.1021/acs.jmedchem.1c01905

Author Contributions

⊥These authors have contributed equally.

Notes

The authors declare no competing financial interest.

■ ACKNOWLEDGMENTS

This project was financed with the NWA Idea generator program (NWA.1228.191.006, NWO, Dutch Research Council). R.C. was financed by the Ramón-Areces Foundation (Spain) and the NACTAR program (Novel Antibacterial Compounds and Therapies Antagonising Resistance, NWO, Project No. 16433).

■ REFERENCES

(1) Prestinaci, F.; Pezzotti, P.; Pantosti, A. Antimicrobial Resistance: A Global Multifaceted Phenomenon. *Pathog. Global Health* **2015**, *109* (7), 309−318.

(2) Ventola, C. L. The Antibiotic Resistance Crisis. *Pharm. Ther.* **2015**, *40* (4), 277−283.

(3) Butler, M. S.; Paterson, D. L. Antibiotics in the Clinical Pipeline in October 2019. *J. Antibiot.* **2020**, *73* (6), 329−364.

(4) Theuretzbacher, U.; Bush, K.; Harbarth, S.; Paul, M.; Rex, J. H.; Tacconelli, E.; Thwaites, G. E. Critical Analysis of Antibacterial Agents in Clinical Development. *Nat. Rev. Microbiol.* **2020**, *18* (5), 286−298.

(5) Theuretzbacher, U.; Outterson, K.; Engel, A.; Karlén, A. The Global Preclinical Antibacterial Pipeline. *Nat. Rev. Microbiol.* **2020**, *18* (5), 275−285.

(6) Theuretzbacher, U.; Bush, K.; Harbarth, S.; Paul, M.; Rex, J. H.; Tacconelli, E.; Thwaites, G. E. Critical Analysis of Antibacterial Agents in Clinical Development. *Nat. Rev. Microbiol.* **2020**, *18* (5), 286−298.
(7) World Health Organization. *Global Priority List of Antibiotic-Resistant Bacteria to Guide Research, Discovery, and Development of New Antibiotics;* World Health Organization, 2017.
(8) Rhodes, D.; Lipps, H. J. G-Quadruplexes and Their Regulatory Roles in Biology. *Nucleic Acids Res.* **2015**, *43* (18), 8627−8637.
(9) Ruggiero, E.; Richter, S. N. G-Quadruplexes and G-Quadruplex Ligands: Targets and Tools in Antiviral Therapy. *Nucleic Acids Res.* **2018**, *46*, 3270−3283.
(10) Cree, S. L.; Kennedy, M. A. Relevance of G-Quadruplex Structures to Pharmacogenetics. *Front. Pharmacol.* **2014**, *5*, 160.
(11) Todd, A. K.; Johnston, M.; Neidle, S. Highly Prevalent Putative Quadruplex Sequence Motifs in Human DNA. *Nucleic Acids Res.* **2005**, *33* (9), 2901−2907.
(12) Amrane, S.; Kerkour, A.; Bedrat, A.; Vialet, B.; Andreola, M.-L.; Mergny, J.-L. Topology of a DNA G-Quadruplex Structure Formed in the HIV-1 Promoter: A Potential Target for Anti-HIV Drug Development. *J. Am. Chem. Soc.* **2014**, *136*, 5249−5252.
(13) Wang, S.-R.; Zhang, Q.-Y.; Wang, J.-Q.; Ge, X.-Y.; Song, Y.-Y.; Wang, Y.-F.; Li, X.-D.; Fu, B.-S.; Xu, G.-H.; Shu, B.; Gong, P.; Zhang, B.; Tian, T.; Zhou, X. Chemical Targeting of a G-Quadruplex RNA in the Ebola Virus L Gene. *Cell Chem. Biol.* **2016**, *23* (9), 1113−1122.
(14) Burge, S.; Parkinson, G. N.; Hazel, P.; Todd, A. K.; Neidle, S. Quadruplex DNA: Sequence, Topology and Structure. *Nucleic Acids Res.* **2006**, *34* (19), 5402−5415.
(15) Balasubramanian, S.; Hurley, L. H.; Neidle, S. Targeting G-Quadruplexes in Gene Promoters: A Novel Anticancer Strategy? *Nat. Rev. Drug Discovery* **2011**, *10*, 261−275.
(16) Onel, B.; Lin, C.; Yang, D. DNA G-Quadruplex and Its Potential as Anticancer Drug Target. *Sci. China: Chem.* **2014**, *57* (12), 1605−1614.
(17) Cimino-Reale, G.; Zaffaroni, N.; Folini, M. Emerging Role of G-Quadruplex DNA as Target in Anticancer Therapy. *Curr. Pharm. Des.* **2017**, *22* (44), 6612−6624.
(18) Métifiot, M.; Amrane, S.; Litvak, S.; Andreola, M.-L. G-Quadruplexes in Viruses: Function and Potential Therapeutic Applications. *Nucleic Acids Res.* **2014**, *42* (20), 12352−12366.
(19) Wang, S.-R.; Min, Y.-Q.; Wang, J.-Q.; Liu, C.-X.; Fu, B.-S.; Wu, F.; Wu, L.-Y.; Qiao, Z.-X.; Song, Y.-Y.; Xu, G.-H.; Wu, Z.-G.; Huang, G.; Peng, N.-F.; Huang, R.; Mao, W.-X.; Peng, S.; Chen, Y.-Q.; Zhu, Y.; Tian, T.; Zhang, X.-L.; Zhou, X. A Highly Conserved G-Rich Consensus Sequence in Hepatitis C Virus Core Gene Represents a New Anti−Hepatitis C Target. *Sci. Adv.* **2016**, *2* (4), e1501535.
(20) Krafčíková, P.; Demkovičová, E.; Víglaský, V. Ebola Virus Derived G-Quadruplexes: Thiazole Orange Interaction. *Biochim. Biophys. Acta, Gen. Subj.* **2017**, *1861* (5), 1321−1328.
(21) Belmonte-Reche, E.; Serrano-Chacón, I.; Gonzalez, C.; Gallo, J.; Bañobre-López, M. Potential G-Quadruplexes and i-Motifs in the SARS-CoV-2. *PLoS One* **2021**, *16* (6), No. e0250654.
(22) Belmonte-Reche, E.; Martínez-García, M.; Guédin, A.; Zuffo, M.; Arévalo-Ruiz, M.; Doria, F.; Campos-Salinas, J.; Maynadier, M.; López-Rubio, J. J.; Freccero, M.; Mergny, J.-L.; Pérez-Victoria, J. M.; Morales, J. C. G-Quadruplex Identification in the Genome of Protozoan Parasites Points to Naphthalene Diimide Ligands as New Antiparasitic Agents. *J. Med. Chem.* **2018**, *61* (3), 1231−1240.
(23) Harris, L. M.; Monsell, K. R.; Noulin, F.; Famodimu, M. T.; Smargiasso, N.; Damblon, C.; Horrocks, P.; Merrick, C. J. G-Quadruplex DNA Motifs in the Malaria Parasite Plasmodium Falciparum and Their Potential as Novel Antimalarial Drug Targets. *Antimicrob. Agents Chemother.* **2018**, *62* (3), e01828−17.
(24) Yadav, P.; Kim, N.; Kumari, M.; Verma, S.; Sharma, T. K.; Yadav, V.; Kumar, A. G-Quadruplex Structures in Bacteria - Biological Relevance and Potential as Antimicrobial Target. *J. Bacteriol.* **2021**, *203*, No. e0057720.
(25) Bartas, M.; Čutová, M.; Brázda, V.; Kaura, P.; Šťastný, J.; Kolomazník, J.; Coufal, J.; Goswami, P.; Červeň, J.; Pečinka, P. The Presence and Localization of G-Quadruplex Forming Sequences in the Domain of Bacteria. *Molecules* **2019**, *24* (9), 1711.
(26) Shao, X.; Zhang, W.; Umar, M. I.; Wong, H. Y.; Seng, Z.; Xie, Y.; Zhang, Y.; Yang, L.; Kwok, C. K.; Deng, X. RNA G-Quadruplex Structures Mediate Gene Regulation in Bacteria. *mBio* **2020**, *11* (1), e02926−19.
(27) Li, Q.; Xiang, J.-F.; Yang, Q.-F.; Sun, H.-X.; Guan, A.-J.; Tang, Y.-L. G4LDB: A Database for Discovering and Studying G-Quadruplex Ligands. *Nucleic Acids Res.* **2013**, *41* (D1), D1115−D1123.
(28) Pirota, V.; Stasi, M.; Benassi, A.; Doria, F. An Overview of Quadruplex Ligands: Their Common Features and Chemotype Diversity. In *Annual Reports in Medicinal Chemistry;* Neidle, S., Ed.; Quadruplex Nucleic Acids As Targets For Medicinal Chemistry; Academic Press, 2020; Vol. *54*, pp 163−196 DOI: 10.1016/bs.armc.2020.04.008.
(29) Pirota, V.; Nadai, M.; Doria, F.; Richter, S. N. Naphthalene Diimides as Multimodal G-Quadruplex-Selective Ligands. *Molecules* **2019**, *24* (3), 426.
(30) Zuffo, M.; Guédin, A.; Leriche, E.-D.; Doria, F.; Pirota, V.; Gabelica, V.; Mergny, J.-L.; Freccero, M. More Is Not Always Better: Finding the Right Trade-off between Affinity and Selectivity of a G-Quadruplex Ligand. *Nucleic Acids Res.* **2018**, *46* (19), e115.
(31) Tassinari, M.; Cimino-Reale, G.; Nadai, M.; Doria, F.; Butovskaya, E.; Recagni, M.; Freccero, M.; Zaffaroni, N.; Richter, S. N.; Folini, M. Down-Regulation of the Androgen Receptor by G-Quadruplex Ligands Sensitizes Castration-Resistant Prostate Cancer Cells to Enzalutamide. *J. Med. Chem.* **2018**, *61* (19), 8625−8638.
(32) Platella, C.; Pirota, V.; Musumeci, D.; Rizzi, F.; Iachettini, S.; Zizza, P.; Biroccio, A.; Freccero, M.; Montesarchio, D.; Doria, F. Trifunctionalized Naphthalene Diimides and Dimeric Analogues as G-Quadruplex-Targeting Anticancer Agents Selected by Affinity Chromatography. *Int. J. Mol. Sci.* **2020**, *21* (6), 1964.
(33) Marchetti, C.; Zyner, K. G.; Ohnmacht, S. A.; Robson, M.; Haider, S. M.; Morton, J. P.; Marsico, G.; Vo, T.; Laughlin-Toth, S.; Ahmed, A. A.; Di Vita, G.; Pazitna, I.; Gunaratnam, M.; Besser, R. J.; Andrade, A. C. G.; Diocou, S.; Pike, J. A.; Tannahill, D.; Pedley, R. B.; Evans, T. R. J.; Wilson, W. D.; Balasubramanian, S.; Neidle, S. Targeting Multiple Effector Pathways in Pancreatic Ductal Adenocarcinoma with a G-Quadruplex-Binding Small Molecule. *J. Med. Chem.* **2018**, *61* (6), 2500−2517.
(34) Ohnmacht, S. A.; Marchetti, C.; Gunaratnam, M.; Besser, R. J.; Haider, S. M.; Di Vita, G.; Lowe, H. L.; Mellinas-Gomez, M.; Diocou, S.; Robson, M.; Šponer, J.; Islam, B.; Barbara Pedley, R.; Hartley, J. A.; Neidle, S. A G-Quadruplex-Binding Compound Showing Anti-Tumour Activity in an in Vivo Model for Pancreatic Cancer. *Sci. Rep.* **2015**, *5*, 11385.
(35) Callegaro, S.; Perrone, R.; Scalabrin, M.; Doria, F.; Palù, G.; Richter, S. N. A Core Extended Naphtalene Diimide G-Quadruplex Ligand Potently Inhibits Herpes Simplex Virus 1 Replication. *Sci. Rep.* **2017**, *7* (1), 2341.
(36) Tassinari, M.; Zuffo, M.; Nadai, M.; Pirota, V.; Sevilla Montalvo, A. C.; Doria, F.; Freccero, M.; Richter, S. N. Selective Targeting of Mutually Exclusive DNA G-Quadruplexes: HIV-1 LTR as Paradigmatic Model. *Nucleic Acids Res.* **2020**, *48* (9), 4627−4642.
(37) Zuffo, M.; Stucchi, A.; Campos-Salinas, J.; Cabello-Donayre, M.; Martínez-García, M.; Belmonte-Reche, E.; Pérez-Victoria, J. M.; Mergny, J. L.; Freccero, M.; Morales, J. C.; Doria, F. Carbohydrate-Naphthalene Diimide Conjugates as Potential Antiparasitic Drugs: Synthesis, Evaluation and Structure-Activity Studies. *Eur. J. Med. Chem.* **2019**, *163*, 54−66.
(38) Belmonte-Reche, E.; Morales, J. C. G4-IM Grinder: When Size and Frequency Matter. G-Quadruplex, i-Motif and Higher Order Structure Search and Analysis Tool. *NAR Genomics Bioinforma.* **2020**, *2*, lqz005.
(39) Faudale, M.; Cogoi, S.; Xodo, L. E. Photoactivated Cationic Alkyl-Substituted Porphyrin Binding to G4-RNA in the 5′-UTR of KRAS Oncogene Represses Translation. *Chem. Commun.* **2012**, *48* (6), 874−876.

(40) Gomez, D.; Guédin, A.; Mergny, J.-L.; Salles, B.; Riou, J.-F.; Teulade-Fichou, M.-P.; Calsou, P. A G-Quadruplex Structure within the 5′-UTR of TRF2MRNA Represses Translation in Human Cells. *Nucleic Acids Res.* **2010**, *38* (20), 7187−7198.
(41) Tran, P. L. T.; Mergny, J.-L.; Alberti, P. Stability of Telomeric G-Quadruplexes. *Nucleic Acids Res.* **2011**, *39* (8), 3282−3294.
(42) Kolesnikova, S.; Hubálek, M.; Bednárová, L.; Cvačka, J.; Curtis, E. A. Multimerization Rules for G-Quadruplexes. *Nucleic Acids Res.* **2017**, *45* (15), 8684−8696.
(43) Varizhuk, A. M.; Protopopova, A. D.; Tsvetkov, V. B.; Barinov, N. A.; Podgorsky, V. V.; Tankevich, M. V.; Vlasenok, M. A.; Severov, V. V.; Smirnov, I. P.; Dubrovin, E. V.; Klinov, D. V.; Pozmogova, G. E. Polymorphism of G4 Associates: From Stacks to Wires via Interlocks. *Nucleic Acids Res.* **2018**, *46* (17), 8978−8992.
(44) Puig Lombardi, E.; Holmes, A.; Verga, D.; Teulade-Fichou, M.-P.; Nicolas, A.; Londoño-Vallejo, A. Thermodynamically Stable and Genetically Unstable G-Quadruplexes Are Depleted in Genomes across Species. *Nucleic Acids Res.* **2019**, *47* (12), 6098−6113.
(45) Arévalo-Ruiz, M.; Doria, F.; Belmonte-Reche, E.; De Rache, A.; Campos-Salinas, J.; Lucas, R.; Falomir, E.; Carda, M.; Pérez-Victoria, J. M.; Mergny, J.-L.; Freccero, M.; Morales, J. C. Synthesis, Binding Properties, and Differences in Cell Uptake of G-Quadruplex Ligands Based on Carbohydrate Naphthalene Diimide Conjugates. *Chem. - Eur. J.* **2017**, *23* (9), 2157−2164.
(46) Doria, F.; Salvati, E.; Pompili, L.; Pirota, V.; D'Angelo, C.; Manoli, F.; Nadai, M.; Richter, S. N.; Biroccio, A.; Manet, I.; Freccero, M. Dyads of G-Quadruplex Ligands Triggering DNA Damage Response and Tumour Cell Growth Inhibition at Subnanomolar Concentration. *Chem. - Eur. J.* **2019**, *25* (47), 11085−11097.
(47) Zuffo, M.; Doria, F.; Botti, S.; Bergamaschi, G.; Freccero, M. G-Quadruplex Fluorescence Sensing by Core-Extended Naphthalene Diimides. *Biochim. Biophys. Acta, Gen. Subj.* **2017**, *1861* (5), 1303−1311.
(48) Pirota, V.; Platella, C.; Musumeci, D.; Benassi, A.; Amato, J.; Pagano, B.; Colombo, G.; Freccero, M.; Doria, F.; Montesarchio, D. On the Binding of Naphthalene Diimides to a Human Telomeric G-Quadruplex Multimer Model. *Int. J. Biol. Macromol.* **2021**, *166*, 1320−1334.
(49) Doria, F.; Nadai, M.; Sattin, G.; Pasotti, L.; Richter, S. N.; Freccero, M. Water Soluble Extended Naphthalene Diimides as PH Fluorescent Sensors and G-Quadruplex Ligands. *Org. Biomol. Chem.* **2012**, *10* (19), 3830−3840.
(50) Committee for Clinical Laboratory Standards. *Methods for Dilution Antimicrobial Susceptibility Tests for Bacteria That Grow Aerobically: M07-A10 ; Approved Standard,* 10th ed.; Clinical and Laboratory Standards Institute: Wayne, PA, 2015.
(51) Sahm, D. F.; Kissinger, J.; Gilmore, M. S.; Murray, P. R.; Mulder, R.; Solliday, J.; Clarke, B. In Vitro Susceptibility Studies of Vancomycin-Resistant Enterococcus Faecalis. *Antimicrob. Agents Chemother.* **1989**, *33* (9), 1588−1591.
(52) Hörner, T.; Zähner, H.; Kellner, R.; Jung, G. Fermentation and Isolation of Epidermin, a Lanthionine Containing Polypeptide Antibiotic from Staphylococcus Epidermidis. *Appl. Microbiol. Biotechnol.* **1989**, *30* (3), 219−225.
(53) Delcour, A. H. Outer Membrane Permeability and Antibiotic Resistance. *Biochim. Biophys. Acta, Proteins Proteomics* **2009**, *1794* (5), 808−816.
(54) Li, Q.; Cebrián, R.; Montalbán-López, M.; Ren, H.; Wu, W.; Kuipers, O. P. Outer-Membrane-Acting Peptides and Lipid II-Targeting Antibiotics Cooperatively Kill Gram-Negative Pathogens. *Commun. Biol.* **2021**, *4* (1), 31.
(55) de Jong, A.; van der Meulen, S.; Kuipers, O. P.; Kok, J. T-REx: Transcriptome Analysis Webserver for RNA-Seq Expression Data. *BMC Genomics* **2015**, *16* (1), 663.
(56) Gu, Z.; Gu, L.; Eils, R.; Schlesner, M.; Brors, B. Circlize Implements and Enhances Circular Visualization in R. *Bioinformatics* **2014**, *30* (19), 2811−2812.
(57) Del Villar-Guerra, R.; Trent, J. O.; Chaires, J. B. G-Quadruplex Secondary Structure Obtained from Circular Dichroism Spectroscopy. *Angew. Chem., Int. Ed.* **2018**, *57* (24), 7171−7175.
(58) Wang, K.; Flaherty, D. P.; Chen, L.; Yang, D. High-Throughput Screening of G-Quadruplex Ligands by FRET Assay. *Methods Mol. Biol.* **2019**, *2035*, 323−331.
(59) Allegra, E.; Titball, R. W.; Carter, J.; Champion, O. L. Galleria Mellonella Larvae Allow the Discrimination of Toxic and Non-Toxic Chemicals. *Chemosphere* **2018**, *198*, 469−472.
(60) Maguire, R.; Duggan, O.; Kavanagh, K. Evaluation of Galleria Mellonella Larvae as an in Vivo Model for Assessing the Relative Toxicity of Food Preservative Agents. *Cell Biol. Toxicol.* **2016**, *32* (3), 209−216.
(61) Yang, H.-F.; Pan, A.-J.; Hu, L.-F.; Liu, Y.-Y.; Cheng, J.; Ye, Y.; Li, J.-B. Galleria Mellonella as an in Vivo Model for Assessing the Efficacy of Antimicrobial Agents against Enterobacter Cloacae Infection. *J. Microbiol. Immunol. Infect.* **2017**, *50* (1), 55−61.
(62) Perrone, R.; Doria, F.; Butovskaya, E.; Frasson, I.; Botti, S.; Scalabrin, M.; Lago, S.; Grande, V.; Nadai, M.; Freccero, M.; Richter, S. N. Synthesis, Binding and Antiviral Properties of Potent Core-Extended Naphthalene Diimides Targeting the HIV-1 Long Terminal Repeat Promoter G-Quadruplexes. *J. Med. Chem.* **2015**, *58* (24), 9639−9652.
(63) Agarwala, R.; Barrett, T.; Beck, J.; Benson, D. A.; Bollin, C.; Bolton, E.; Bourexis, D.; Brister, J. R.; Bryant, S. H.; Canese, K.; Cavanaugh, M.; Charowhas, C.; Clark, K.; Dondoshansky, I.; Feolo, M.; Fitzpatrick, L.; Funk, K.; Geer, L. Y.; Gorelenkov, V.; Graeff, A.; Hlavina, W.; Holmes, B.; Johnson, M.; Kattman, B.; Khotomlianski, V.; Kimchi, A.; Kimelman, M.; Kimura, M.; Kitts, P.; Klimke, W.; Kotliarov, A.; Krasnov, S.; Kuznetsov, A.; Landrum, M. J.; Landsman, D.; Lathrop, S.; Lee, J. M.; Leubsdorf, C.; Lu, Z.; Madden, T. L.; Marchler-Bauer, A.; Malheiro, A.; Meric, P.; Karsch-Mizrachi, I.; Mnev, A.; Murphy, T.; Orris, R.; Ostell, J.; O'Sullivan, C.; Palanigobu, V.; Panchenko, A. R.; Phan, L.; Pierov, B.; Pruitt, K. D.; Rodarmer, K.; Sayers, E. W.; Schneider, V.; Schoch, C. L.; Schuler, G. D.; Sherry, S. T.; Siyan, K.; Soboleva, A.; Soussov, V.; Starchenko, G.; Tatusova, T. A.; Thibaud-Nissen, F.; Todorov, K.; Trawick, B. W.; Vakatov, D.; Ward, M.; Yaschenko, E.; Zasypkin, A.; Zbicz, K. Database Resources of the National Center for Biotechnology Information. *Nucleic Acids Res.* **2018**, *46* (D1), D8−D13.
(64) Bedrat, A.; Lacroix, L.; Mergny, J.-L. Re-Evaluation of G-Quadruplex Propensity with G4Hunter. *Nucleic Acids Res.* **2016**, *44* (4), 1746−1759.
(65) Hon, J.; Martínek, T.; Zendulka, J.; Lexa, M. Pqsfinder: An Exhaustive and Imperfection-Tolerant Search Tool for Potential Quadruplex-Forming Sequences in R. *Bioinformatics* **2017**, *33* (21), 3373−3379.
(66) Guédin, A.; Gros, J.; Alberti, P.; Mergny, J. L. How Long Is Too Long? Effects of Loop Size on G-Quadruplex Stability. *Nucleic Acids Res.* **2010**, *38* (21), 7858−7868.
(67) Hernandez-Valdes, J. A.; Aan de Stegge, M.; Hermans, J.; Teunis, J.; van Tatenhove-Pel, R. J.; Teusink, B.; Bachmann, H.; Kuipers, O. P. Enhancement of Amino Acid Production and Secretion by Lactococcus Lactis Using a Droplet-Based Biosensing and Selection System. *Metab. Eng. Commun.* **2020**, *11*, No. e00133.
(68) Goel, A.; Santos, F.; de Vos, W. M.; Teusink, B.; Molenaar, D. Standardized Assay Medium to Measure Lactococcus Lactis Enzyme Activities While Mimicking Intracellular Conditions. *Appl. Environ. Microbiol.* **2012**, *78* (1), 134−143.
(69) Schindelin, J.; Arganda-Carreras, I.; Frise, E.; Kaynig, V.; Longair, M.; Pietzsch, T.; Preibisch, S.; Rueden, C.; Saalfeld, S.; Schmid, B.; Tinevez, J.-Y.; White, D. J.; Hartenstein, V.; Eliceiri, K.; Tomancak, P.; Cardona, A. Fiji: An Open-Source Platform for Biological-Image Analysis. *Nat. Methods* **2012**, *9* (7), 676−682.
(70) Aranda, P. S.; LaJoie, D. M.; Jorcyk, C. L. Bleach Gel: A Simple Agarose Gel for Analyzing RNA Quality. *Electrophoresis* **2012**, *33*, 366−369.
(71) Langmead, B.; Salzberg, S. L. Fast Gapped-Read Alignment with Bowtie 2. *Nat. Methods* **2012**, *9* (4), 357−359.

https://doi.org/10.1021/acs.jmedchem.1c01905
J. Med. Chem. 2022, 65, 4752−4766

(72) Li, H.; Handsaker, B.; Wysoker, A.; Fennell, T.; Ruan, J.; Homer, N.; Marth, G.; Abecasis, G.; Durbin, R. 1000 Genome Project Data Processing Subgroup. The Sequence Alignment/Map Format and SAMtools. *Bioinformatics* **2009**, *25* (16), 2078−2079.
(73) Liao, Y.; Smyth, G. K.; Shi, W. FeatureCounts: An Efficient General Purpose Program for Assigning Sequence Reads to Genomic Features. *Bioinformatics* **2014**, *30* (7), 923−930.
(74) Greenfield, N. J. Using Circular Dichroism Collected as a Function of Temperature to Determine the Thermodynamics of Protein Unfolding and Binding Interactions. *Nat. Protoc.* **2006**, *1* (6), 2527−2535.
(75) Cé, R.; Silva, R. C.; Trentin, D. S.; Marchi, J. G. B. D.; Paese, K.; Guterres, S. S.; Macedo, A. J.; Pohlmann, A. R. Galleria Mellonella Larvae as an In Vivo Model to Evaluate the Toxicity of Polymeric Nanocapsules. *J. Nanosci. Nanotechnol.* **2020**, *20* (3), 1486−1494.
(76) Cutuli, M. A.; Petronio Petronio, G.; Vergalito, F.; Magnifico, I.; Pietrangelo, L.; Venditti, N.; Di Marco, R. Galleria Mellonella as a Consolidated in Vivo Model Hosts: New Developments in Antibacterial Strategies and Novel Drug Testing. *Virulence* **2019**, *10* (1), 527−541.
(77) Ignasiak, K.; Maxwell, A. Galleria Mellonella (Greater Wax Moth) Larvae as a Model for Antibiotic Susceptibility Testing and Acute Toxicity Trials. *BMC Res. Notes* **2017**, *10*, 428.

https://doi.org/10.1021/acs.jmedchem.1c01905
J. Med. Chem. 2022, 65, 4752−4766